A&A manuscript no.
(will be inserted by hand later)

Your thesaurus codes are:
04(08.03.4;08.13.2;08.16.4;13.19.5)

ASTRONOMY AND ASTROPHYSICS

Millimeter and some near infra-red observations of short-period Miras and other AGB stars *

M.A.T. Groenewegen[1], F. Baas[2], J.A.D.L. Blommaert[3], R. Stehle[4], E. Josselin[5], and R.P.J. Tilanus[2]

[1] Max-Planck Institut für Astrophysik, Karl-Schwarzschild-Straße 1, D-85740 Garching, Germany
[2] Joint Astronomy Centre, 660 N. A'ohōkū Place, University Park, Hilo, HI 96720, U.S.A
[3] ISO Data Centre, Astrophysics Division of ESA, P.O. Box 50727, E-28080 Villafranca-Madrid, Spain
[4] Department of Physics & Astronomy, University of Leicester, University Road, Leicester LE1 7RH, United Kingdom
[5] Observatorio Astronómico Nacional (I.G.N.), Apartado 1143, E-28801 Alcalá de Henares, Spain

received, accepted

Abstract. Millimeter observations of 48 oxygen- and 20 carbon-rich AGB Miras with periods shorter than 400 days are presented. In addition, observations of 14 O-rich and 15 C-stars with longer, or no known, periods have also been obtained.

The detection statistics is as follows: in ^{12}CO J=1-0 and 2-1 we observed 97 stars, and detected 66 in at least one line. We find 24 new detections in the 1-0 line, 38 new detections in the 2-1 line, and 29 stars have been detected for the first time in one or both lines. In ^{12}CO J=3-2 we observed 14 stars and detected 11, with 4 new detections. In ^{13}CO J=2-1, 3-2 we observed 2 stars and had one new detection. In HCN(1-0) we observed 5 carbon stars and detected 3, one new. In SO(6_5-5_4) we observed the same 5 stars and detected none. In CS(3-2) we observed 8 carbon stars and detected 3, all new. In SiO(3-2, v=0) we observed 34 O-rich stars and detected 25, all new except one.

Near-infrared JHK photometry is presented for seven stars. For four stars it is the first NIR data published.

The luminosity and dust mass loss rate are obtained for seven very red stars with unknown pulsation period from modelling the spectral energy distribution (SED) and IRAS LRS spectra. Thereby, a new IR supergiant is confirmed (AFGL 2968). For the rest of the sample, luminosity and distance are obtained in a variety of ways: using HIPPARCOS parallaxes, period-luminosity and period-$M_{\rm K}$-relations combined with apparent K magnitudes, and kinematic distances.

The dust mass loss rate is obtained from model fitting of the SED (either from the literature, or presented in the present paper), or from the observed IRAS 60 μm flux, corrected for the photospheric contribution. The gas mass loss rate is derived from the observed CO line intensities, as presented here, combined with existing literature data, if any. This allows the derivation of the dust-to-gas ratio. Our and literature CO J = 3-2 data has been used to calibrate the relation between mass loss rate and peak intensity of the CO(3-2) line.

Diagrams showing mass loss rate, dust-to-gas ratio and expansion velocity versus pulsation period are presented. Our observations confirm the existence of an upper limit for the expansion velocity of C- and O-rich stars, and that this maximum is larger for C-stars, as predicted by the theory of radiation pressure on dust particles.

Key words: circumstellar matter – stars: mass loss – stars: AGB – radio lines: stars

1. Introduction

Previous studies have shown that mass loss rates increase with increasing pulsation periods in Miras. For example, Whitelock (1990) and Whitelock et al. (1994) derived the mass loss rates for oxygen-rich Miras in the Galactic Bulge and the South Galactic Cap, respectively, and found this trend. The mass loss rates were based on dust emission and then converted to a total mass loss rate based on a constant dust-to-gas ratio and expansion velocity for all stars in their respective samples.

In a different approach to derive the dust mass loss rate, Groenewegen et al. (1998) fitted the Spectral Energy

Send offprint requests to: Martin Groenewegen (groen@mpa-garching.mpg.de)

* The James Clerk Maxwell Telescope is operated by the Observatories on behalf of the Science and Engineering Council of the United Kingdom, the Netherlands Organization for Scientific Research, and the National Research Council of Canada. Based on observations made with the Carlos Sanchez telescope operated on the island of Tenerife in the Spanish Observatorio del Teide of the Instituto de Astrofísica de Canarias. Based on observations collected at the European Southern Observatory, La Silla, Chile within programs ESO 57.E-0105, 59.E-0198 and 61.E-0254. Based on data from the ESA Hipparcos astrometry satellite.

Distributions (SEDs) and mid-infrared IRAS LRS spectra of 44 carbon Mira variables with a dust radiative transfer model. In that paper the total mass loss rate was then derived from a modified relation between the photon momentum transfer rate (L/c) and the momentum transfer rate of the wind ($\dot{M}\ v_{\infty}$).

There is an alternative method to derive the total mass loss rate and that is through molecular emission lines, notably CO which is the most abundant molecule after H_2. Many CO observations have been published for AGB stars over the past years (see Loup et al. (1993) for a compilation up to that epoch; more recent work include Bieging & Latter (1994), Sahai & Liechti (1995), Young (1995), Groenewegen et al. (1996), Knapp et al. (1998), Olofsson et al. (1998), Neri et al. (1998), Kerschbaum & Olofsson (1998), Groenewegen & de Jong (1998)). CO observations are the main focus here as well. As the results in Groenewegen et al. (1998) suggested that the overall good relation between mass loss rate and pulsation period might break down for periods shorter than about 400 days we concentrated on the shorter period range, and also included both O- and C-rich Miras. This possible breakdown of a mass loss–period relation might be related to the fact that radiation pressure on dust is no longer sufficient to drive the mass loss at lower luminosity (Dominik et al. 1990).

The paper is organised as follows. In Sect. 2 the sample of stars is introduced and the millimeter observations are described. In Sect. 3 the line profiles and observational results are presented. In Sect. 4 the infrared observations are described. In Sect. 5 the analysis is performed, which includes the modelling of the SEDs and LRS spectra for 7 stars, estimation of luminosity and distance using several methods, derivation of the dust- and gas- mass loss rate. In Sect. 6 we comment on the various correlations between mass loss rate and pulsation period, expansion velocity, etc.

2. The observations

Observations were performed with the IRAM-30m-telescope and the SEST each on three different occasions and with the JCMT on one occasion. In Table 1 we list the observations of the different runs, the observed coordinates, chemical type (C or M) and pulsation period. In addition, references are given to previous detections in CO and in the case of non-detections (previously and by us) we refer to radial velocities obtained by other means, if avaialable. The stellar coordinates are in most cases taken from the SIMBAD data base (when listed to $\lesssim 0.2''$ accuracy), the Hipparcos input catalog, the Stephenson (1989) catalog of carbon stars, or derived from the Digitised Sky Survey. In few cases the IRAS coordinates are used, mostly for the less known carbon stars and the stars listed under their IRAS name. The pulsation periods are taken from the 4th edition of the General Catalog of Variable Stars (GCVS, Kholopov et al. 1985), Jones et al. (1990), Le Bertre (1992) and Joyce et al. (1999).

The data obtained with the IRAM-30m-telescope were taken in the period between 23 and 29 December 1994, between 26 and 28 January 1995 and on the 3rd and 4th of August 1995. For the December 1994 run (observers MG and JB) the ^{12}CO J = 1-0 and J = 2-1 lines, and for some stars also the HCN(1-0) and SO(6_5-5_4) lines, were observed simultaneously using the 230 GHz and 3 mm SIS receivers. Both the two 1MHz filter banks and the autocorrelator were used as backends. In cases where both data sets are available with good S/N we only present the one with the highest frequency resolution. The same procedure is adopted for the other observations discussed below. Table 3 gives the channel spacing which we finally decided to use.

The targets were observed using wobbler switching during all runs with the IRAM-30m-telescope, mostly with a throw of $120''$ in azimuth.

Baselines were removed and all temperatures are on a main-beam brightness scale (the same applies for all temperatures presented in this paper). Due to different definitions used at different telescopes the observed antenna temperatures ($T_{\rm A}$) are converted to main-beam brightness temperatures ($T_{\rm mb}$) by using $T_{\rm mb} = T_{\rm A}/B_{\rm eff}$ for the SEST and JCMT data (discussed below), and $T_{\rm mb} = T_{\rm A} \times F_{\rm eff}/B_{\rm eff}$ for the IRAM data, where $F_{\rm eff}$ and $B_{\rm eff}$ are respectively the forward and main-beam efficiencies (listed in Table 2 together with the FWHM beam widths).

The comparison with the calibration sources (supplemented by consistency checks from stars observed during more days, or even observed both in the December and January runs, as well as published results obtained with the IRAM-30m-telescope) indicated that the CO J = 1-0 and the HCN observations during the December 1994 run are consistent with the calibration observations. The situation is different for the CO J = 2-1 and SO data. The observed CO J = 2-1 data had to be multiplied by factors 1.1 - 1.5 to obtain agreement with previous results. For the SO transitions there are no calibration sources and only very few published data. The 230 GHz receiver was tuned to the SO line during two consecutive days during the December 1994 run. We observed IRC+10 011 on both days and compared our data to that of Bujarrabal et al. (1994). On the first day our brightness temperature scale was too low by a factor of 2.2; on the second day we found agreement between the two. By scaling the result for VY CMa obtained with the NRAO 12m telescope to the expected value for the IRAM-30m-telescope, assuming a point source, we again found an underestimate of the temperature scale by a factor of 2.2 for the first day of SO observations. Hence, for the first day of SO observations the observed brightness temperatures were multiplied by 2.2; for the second day no correction was applied. We estimate the final calibration for all observed lines to

Table 1. The sample

Name	R.A. (1950)	Dec. (1950)	Type	Period (days)	References
			IRAM December 1994 run		
V390 Cas	01 25 16.3	+62 01 09	C	362[a]	
PT Cas	01 34 51.5	+55 42 56	C	300	
CN Per	02 03 12.7	+56 36 43	C	384	
R For	02 27 01.31	−26 19 14.8	C	388.7	Loup et al. (1993), Olofsson et al. (1993, 1998)
AFGL 5076	02 34 34.6	+54 22 19	C	–	Volk et al. (1993)
IRAS 02408+5458	02 40 49.1	+54 58 35	C	–	
GY Per	04 25 50.76	+39 27 11.2	C	377.8	
UV Aur	05 18 33.31	+32 27 51.4	C	394.2[b]	SIMBAD
ZZ Gem	06 20 56.5	+25 03 31	C	317.0	
AFGL 935	06 23 04.64	−09 30 20.1	C	494	Loup et al. (1993)
IRAS 06582+1507	06 58 17.3	+15 07 58	C	–	Loup et al. (1993), Volk et al. (1993)
R CMi	07 05 57.56	+10 06 16.1	C	337.8	SIMBAD
VX Gem	07 09 58.6	+14 41 11	C	379.4	SIMBAD
C1698	07 22 09.3	−04 31 58	C	–	Engels (1994)
R Pyx	08 43 23.8	−28 01 04	C	364.7	
V CrB	15 47 43.89	+39 43 20.5	C	357.6	Loup et al. (1993), Olofsson et al. (1993), Knapp et al. (1998), Neri et al. (1998)
V Oph	16 23 56.58	−12 18 54.7	C	297.2	
AFGL 2310	19 00 53.05	+07 26 21.9	C	577	Loup et al. (1993), Likkel & Miao (1996)
AFGL 2368	19 17 35.39	−08 07 51.0	C	676	Loup et al. (1993)
AFGL 2686	20 57 00.28	+27 14 51.4	C	750	Loup et al. (1993)
V1549 Cyg	21 03 32.6	+51 36 18	C	533	Loup et al. (1993)
AX Cep	21 26 15.0	+70 00 16	C	395.0	
AFGL 5625	21 31 50.1	+56 31 13	C	–	Loup et al. (1993), Volk et al. (1993), Neri et al. (1998)
CIT 13	21 32 06.06	+38 50 52.9	C	470	Loup et al. (1993), Olofsson et al. (1993)
AO Lac	22 40 35.9	+51 15 36	C	300	
LS Cas	23 35 45.8	+55 45 12	C	340	
AFGL 230	01 30 27.63	+62 11 31.2	O	1525	Loup et al. (1993), Neri et al. (1998)
AFGL 5093	03 20 41.48	+65 21 32.8	O	1276	Loup et al. (1993)
AFGL 5097	03 29 23.65	+60 10 04.4	O	–	Loup et al. (1993)
NV Aur	05 07 19.68	+52 48 53.9	O	635	Loup et al. (1993)
AFGL 712	05 13 06.6	+45 30 48	O	1088	
IRAS 05284+1945	05 28 27.2	+19 45 08	O	–	
IRAS 06403−0138	06 40 19.1	−01 38 05	O	–	
IRAS 07113−2747	07 11 23.1	−27 47 46	O	–	
OH 10.1−0.1	18 05 17.95	−20 16 41.0	O	–	Blommaert et al. (1994)
IRAS 21554+6204	21 55 29.6	+62 04 24	O	–	Loup et al. (1993)
AFGL 2885	22 17 42.7	+59 36 17	O	1570	Loup et al. (1993)
AFGL 2968	22 48 00.9	+60 02 01	O	–	Josselin et al. (1998)
			IRAM January 1995 run		
Y Per	03 24 18.07	+44 00 12.6	C	248.6	
R Ori	04 56 17.62	+08 03 19.7	C	377.1	
V Aur	06 20 15.4	+47 44 03	C	353.0	
ZZ Gem	06 20 56.5	+25 03 31	C	317.0	
R CMi	07 05 57.56	+10 06 16.1	C	337.8	
R Pyx	08 43 23.8	−28 01 04	C	364.7	
V CrB	15 47 43.89	+39 43 20.5	C	357.6	see above
V Oph	16 23 56.58	−12 18 54.7	C	297.2	
AX Cep	21 26 15.0	+70 00 16	C	395.0	
U Ori	05 52 50.95	+20 10 08.1	O	368.3	Young (1995), Knapp et al. (1998)
R LMi	09 42 34.75	+34 44 33.9	O	372.2	Loup et al. (1993), Young (1995)
R Leo	09 44 52.22	+11 39 42.0	O	310.0	Loup et al. (1993), Bieging & Latter (1994), Young (1995), Stanek et al. (1995), Olofsson et al. (1998)
RS Vir	14 24 46.00	+04 54 06.3	O	354.0	
R Ser	15 48 23.26	+15 17 03.1	O	356.4	Loup et al. (1993), Young (1995), Knapp et al. (1998)
X Oph	18 35 57.57	+08 47 19.9	O	328.9	Young (1995)
R Peg	23 04 08.27	+10 16 22.8	O	378.1	Young (1995)

Table 1. Continued

Name	R.A. (1950)	Dec. (1950)	Type	Period (days)	References
				IRAM August 1995 run	
R Cet	02 23 28.71	−00 24 11.0	O	166.2	
R Tri	02 34 00.02	+34 02 51.6	O	266.9	SIMBAD
R Tau	04 25 33.46	+10 03 08.9	O	320.9	
T Lep	05 02 43.20	−21 58 18.7	O	368.1	
X Hya	09 33 06.94	−14 28 03.5	O	301.1	Young (1995)
R Aqr	23 41 14.18	−15 33 41.8	O	387.0	
				JCMT August 1995 run	
R For	02 27 01.31	−26 19 14.8	C	388.7	see above
UV Aur	05 18 33.31	+32 27 51.4	C	394.2	see above
R Cap	20 08 30.18	−14 25 02.3	C	345.1	
AX Cep	21 26 15.0	+70 00 16	C	395.0	
S Scl	00 12 51.11	−32 19 22.5	O	362.7	Cho et al. (1996), Haikala (1990)
R Cet	02 23 28.71	−00 24 11.0	O	166.2	
RT Eri	03 31 54.33	−16 19 51.1	O	370.8	
W Eri	04 09 25.24	−25 15 43.3	O	376.6	
RS Eri	04 15 41.82	−18 37 42.8	O	296.0	Lewis (1997)
R Tau	04 25 33.46	+10 03 08.9	O	320.9	
BD Eri	04 31 11.28	−00 04 37.6	O	336	Benson & Little-Marenin (1996)
T Lep	05 02 43.20	−21 58 18.7	O	368.1	
U Ori	05 52 50.95	+20 10 08.1	O	368.3	see above
X Oph	18 35 57.57	+08 47 19.9	O	328.9	see above
RT Aql	19 35 40.42	+11 36 27.6	O	327.1	Young (1995)
BG Cyg	19 36 56.87	+28 23 51.4	O	419.8[c]	
Z Cyg	20 00 02.6	+49 54 07	O	263.7	Young (1995), Josselin et al. (1998)
RU Cap	20 29 39.36	−21 51 39.6	O	347.4	
TU Peg	21 42 39.21	+12 28 05.1	O	321.6	
R Peg	23 04 08.27	+10 16 22.8	O	378.1	see above
W Peg	23 17 22.65	+26 00 18.4	O	345.5	Young (1995)
R Aqr	23 41 14.18	−15 33 41.8	O	387.0	
				SEST September 1996 run	
AFGL 971	06 34 16.4	+03 28 05	C	653	Loup et al. (1993), Knapp et al. (1998)
CL Mon	06 52 55.9	+06 26 37	C	497.2	Loup et al. (1993), Olofsson et al. (1993), Neri et al. (1998)
R CMi	07 05 57.56	+10 06 16.1	C	337.8	
R Vol	07 06 32.6	−72 56 01	C	453.6	Loup et al. (1993), Olofsson et al. (1993, 1998)
R Pyx	08 43 23.8	−28 01 04	C	364.7	
V Cru	12 53 36.64	−57 37 44.1	C	376.5	
R Cap	20 08 30.18	−14 25 02.3	C	345.1	
RZ Peg	22 03 39.05	+33 15 39.7	C	438.7	SIMBAD
o Cet	02 16 49.05	−03 12 13.4	O	332.0	Loup et al. (1993), Young (1995), Bujarrabal et al. (1994), Stanek et al. (1995), Knapp et al. (1998)
U Ari	03 08 16.56	+14 36 41.9	O	371.1	Young (1995)
RT Eri	03 31 54.33	−16 19 51.1	O	370.8	
U Hor	03 51 11.83	−45 58 40.3	O	348.4	Haikala et al. (1994)
W Eri	04 09 25.24	−25 15 43.3	O	376.6	
R Tau	04 25 33.46	+10 03 08.9	O	320.9	
RX Tau	04 35 31.75	+08 14 13.9	O	331.8	Duflot et al. (1995)
R Cae	04 38 45.87	−38 19 51.3	O	391.0	Haikala et al. (1994)
T Lep	05 02 43.20	−21 58 18.7	O	368.1	
U Dor	05 09 50.90	−64 22 42.6	O	394.4	Loup et al. (1993)
RT Lep	05 40 28.76	−23 43 02.7	O	399.0	
U Ori	05 52 50.95	+20 10 08.1	O	368.3	see above
AS Pup	08 07 50.32	−38 01 34.7	O	324.7	Haikala et al. (1994)
R Car	09 30 59.21	−62 34 01.1	O	308.7	
W Vel	10 13 22.67	−54 13 44.8	O	394.7	

Table 1. Continued

Name	R.A. (1950)	Dec. (1950)	Type	Period (days)	References
RZ Mus	12 57 30.64	−70 41 35.3	O	333.7	
AQ Cen	14 02 01.96	−35 15 31.8	O	387.5	
RU Hya	14 08 40.87	−28 39 01.0	O	331.5	
Y Lup	14 55 56.79	−54 46 02.7	O	396.8	
S Ser	15 19 18.97	+14 29 35.0	O	371.8	
RS Lib	15 21 24.28	−22 44 05.4	O	217.7	Young (1995)
BG Ser	15 41 01.46	−01 33 11.7	O	143[d]	
R Ser	15 48 23.26	+15 17 03.1	O	356.4	see above
RR Sco	16 53 26.31	−30 30 08.3	O	281.5	Young (1995)
RW Sco	17 11 34.82	−33 22 32.5	O	388.5	
V545 Oph	17 36 43.78	−23 19 49.4	O	223	
V438 Sco	17 53 51.45	−37 28 41.3	O	392.0	
WY Her	17 57 59.53	+23 35 41.3	O	376	
X Oph	18 35 57.57	+08 47 19.9	O	328.9	see above
V342 Sgr	19 09 21.19	−32 56 05.4	O	372	Loup et al. (1993)
W Aql	19 12 41.6	−07 08 08	O	490.4	Loup et al. (1993), Bieging & Latter (1994), Sahai & Liechti (1994), Bieging et al. (1999), Knapp et al. (1998)
RT Aql	19 35 40.42	+11 36 27.6	O	327.1	see above
RR Sgr	19 52 49.89	−29 19 23.6	O	336.3	
RR Aql	19 55 00.41	−02 01 17.5	O	394.8	Loup et al. (1993), Olofsson et al. (1998)
				SEST September 1997 run	
RZ Peg	22 03 39.05	+33 15 39.7	C	438.7	
o Cet	02 16 49.05	−03 12 13.4	O	332.0	see above
RT Eri	03 31 54.33	−16 19 51.1	O	370.8	
AQ Cen	14 02 01.96	−35 15 31.8	O	387.5	
Y Lup	14 55 56.79	−54 46 02.7	O	396.8	
RR Sco	16 53 26.31	−30 30 08.3	O	281.5	see above
RW Sco	17 11 34.82	−33 22 32.5	O	388.5	
V438 Sco	17 53 51.45	−37 28 41.3	O	392.0	
V342 Sgr	19 09 21.19	−32 56 05.4	O	372	see above
RR Sgr	19 52 49.89	−29 19 23.6	O	336.3	
RR Aql	19 55 00.41	−02 01 17.5	O	394.8	see above
				SEST September 1998 run	
AFGL 971	06 34 16.4	+03 28 05	C	653.	see above
R Vol	07 06 32.6	−72 56 01	C	453.6	see above
R Cap	20 08 30.18	−14 25 02.3	C	345.1	
U Ari	03 08 16.56	+14 36 41.9	O	371.1	see above
W Eri	04 09 25.24	−25 15 43.3	O	376.6	
R Tau	04 25 33.46	+10 03 08.9	O	320.9	
RX Tau	04 35 31.75	+08 14 13.9	O	331.8	
T Lep	05 02 43.20	−21 58 18.7	O	368.1	
U Dor	05 09 50.90	−64 22 42.6	O	394.4	
U Ori	05 52 50.95	+20 10 08.1	O	368.3	see above
R Car	09 30 59.21	−62 34 01.1	O	308.7	
W Vel	10 13 22.67	−54 13 44.8	O	394.7	
RZ Mus	12 57 30.64	−70 41 35.3	O	333.7	
AQ Cen	14 02 01.96	−35 15 31.8	O	387.5	
Y Lup	14 55 56.79	−54 46 02.7	O	396.8	
V545 Oph	17 36 43.78	−23 19 49.4	O	223	
X Oph	18 35 57.57	+08 47 19.9	O	328.9	see above

Notes. (a) Currently (Nov. 1998) listed in SIMBAD as a possibly Semi-Regular (SR) without period. (b) Currently listed in SIMBAD as a SR with a period of 393.4 days. (c) Currently listed in SIMBAD with a period of 291 days ! The HIPPARCOS output catalog (ESA 1997) lists a period of 287.3 days. (d) The HIPPARCOS output catalog lists a period of 404 days.
Comparing the SIMBAD database with the periods listed in the 4th edition of the GCVS shows that there are four stars for which the periods changed by more than 4 days: AX Cep (399.1), U Ori (372.5), X Oph (334.2) and Y Lup (402.1).
Some stars have been assigned variable star names (as of Nov. 1998): AFGL 230 (V669 Cas), AFGL 935 (V713 Mon), AFGL 971 (V688 Mon), AFGL 2310 (V1418 Aql), AFGL 2368 (V1420 Aql), CIT 13 (V1426 Cyg).

be accurate by about 10% (1σ). This is true for all runs with the IRAM-30m-telescope.

For the January 1995 run (Observer MG) the ^{12}CO J = 1-0, 2-1 and 3-2 transitions were observed simultaneously with three SIS receivers. We used as backends the 1MHz filterbank and the autocorrelator, which was split into three parts. The data reduction is similar as described above. For the J = 3-2 line there were at that time no calibration observations available for the IRAM-30m-telescope.

For the August 1995 run (observer EJ) the ^{12}CO J = 1-0, 2-1 transitions were observed simultaneously, in a set-up identical to the December 1994 run.

The JCMT data were taken on August 28 and September 1 & 7, 1995 (observers FB and RT). The ^{12}CO J = 2-1, J = 3-2 and, for a subsample, ^{13}CO J = 2-1 and J = 3-2 were observed using two SIS receivers. The backend was the digital autocorrelation spectrometer. A chopping secondary was used with a throw of $2'$. The data reduction is similar as described above. We estimate the calibration to be accurate to about 10% (1σ).

The first set of SEST data was taken between 11 and 16 September 1996 (observer MG). Either ^{12}CO J = 1-0 and SiO (3-2, v=0), or ^{12}CO J = 1-0 and CS (3-2) were observed simultaneously using the 2mm and 3mm SIS receivers. The former setting was used to observe O-rich sources, and the latter was used for the C-rich sources. This was not our preferred set-up but the 1.3mm receiver was unavailable during our run to observe the CO (2-1) line. The dual beam switching mode was used with a throw of $2'26''$ in azimuth. One of two available acousto-optical spectrometers was split and connected to the two receivers with a channel separation of 0.7 MHz.

During the second (20-21 September 1997; observer RS) and third (30 September 1998; observer MG) SEST run the ^{12}CO J = 1-0 and 2-1 lines were observed simultaneously with the 1.3mm and 3mm SIS receivers using the dual beam switching mode as outlined above. We targeted only those stars which had already been detected in the 1996 September run. The data reduction for the SEST runs is similar as described above. Based on a comparison with calibration sources we estimate the brightness temperature scale to be accurate to about 10% (1σ)

3. Results of the observations

Table 3 lists the results of the observing run. Included are the name of the object, the transition, the channel spacing, the rms noise, the peak temperature, the integrated intensity, the central velocity with respect to the local standard of rest and half the velocity width at zero intensity which equals the expansion velocity of the circumstellar shell. These quantities were determined either directly from the profiles or from profile fits using the reduction program CLASS (Forveille et al. 1990). Typical 1σ uncertainties in the central velocity and the expansion velocity are 1 km s^{-1}. The 1σ uncertainties in the peak temperature and the integrated intensity are dominated by the calibration uncertainties. Values flagged with a colon are particularly uncertain. Upper limits are 3σ values.

Data of stars observed with the IRAM-30m-telescope on two separate occasions are co-added first. The results are also included in Table 3. For ZZ Gem we only co-added the CO (2-1) spectra as the CO (1-0) line was detected on only one occasion; for R Pyx only the December 1994 data is used, as the integration time during the January 1995 run was only three minutes, resulting in a poor signal-to-noise level. For AX Cep only the January 1995 data is used, as the CO (2-1) emission is much stronger, and the peak of strongest emission was found to be at a slight offset compared to the position observed in December 1994.

Data obtained with SEST were also co-added, and only the final results are included in Table 3. In the cases where the CO (1-0) line was detected on two or three occasions, the observed temperatures were in good agreement within the limits of the observation. Also observations of CO (1-0) and (2-1) calibrator stars on different occasions were in agreement with each other.

For stars without detection the stellar LSR velocity is listed in brackets when available. References are listed in Table 1. When this is "SIMBAD" it is an optical velocity as listed in the "oRV" field, transformed to the LSR frame. When several significantly different values are listed by SIMBAD, the range is given.

The calibrated profiles are shown in the Figs. 1-3 (carbon stars) and 4-9 (oxygen-rich stars). A velocity range of 100 km s^{-1} is plotted, centered on the system velocity. Stars not detected in any of the observed lines are not shown. Stars observed with different telescopes are shown separately. The figures are arranged by increasing right ascension.

The line shapes of the profiles are that typical of AGB stars, that is parabolic (e.g. R For in Fig. 1, U Dor in Fig. 5 of AFGL 2968 in Fig. 8), or flat-topped (e.g. AFGL 2310 in Fig. 2). Some lineprofiles are affected by interstellar emission or absorption (e.g. AFGL 971 in Fig. 2, and AFGL 5625 and V1548 Cyg in Fig. 3). The most unusual shaped line profile is that of AFGL 2368 (Fig. 3), which shows a clear asymmetrical profile, inparticular in the 1-0 line. A SEST CO (1-0) observation (Nyman et al. 1992) does not seem to show this, but there is a hint of a similar asymmetrical line shape in an CO (1-0) observation with the FCRAO (Margulis et al. 1990).

4. Near-infrared observations

We obtained JHK photometry for a few stars with the 1.5m Carlos Sanchez telescope at the Teide observatory on the island of Tenerife. A single-channel infrared photometer was used with an aperture of $15''$. Cycles of 'on-off-on'

Table 3. The observed quantities

name	transition	Δv (km s^{-1})	rms (K)	$T_{\rm peak}$ (K)	$\int T$ dv (K km s^{-1})	v$_{\rm c}$ (km s^{-1})	v$_{\rm e}$ (km s^{-1})	remarks
			IRAM December 1994 run					
			C-stars					
V390 Cas	1-0	2.60	0.018	–	–	–	–	
	2-1	1.30	0.038	–	–	–	–	
PT Cas	1-0	2.60	0.028	–	–	–	–	
	2-1	1.30	0.050	–	–	–	–	
CN Per	1-0	2.60	0.020	–	–	–	–	
	2-1	1.30	0.031	–	–	–	–	
R For	1-0	1.63	0.034	0.38	11.4 ± 0.3	–1.7	16.9	
	2-1	0.81	0.072	1.62	43.3 ± 0.5	–2.2	16.9	
AFGL 5076	1-0	1.63	0.037	0.63	16.8 ± 0.3	–66.3	20.9	
	2-1	0.81	0.048	1.22	30.2 ± 0.3	–66.8	19.1	
	HCN	2.11	0.019	0.14	3.1 ± 0.2	–64.0	16.8	
	SO	1.36	0.040	–	<2.5	–	–	
IRAS 02408+5458	1-0	2.60	0.023	0.25	4.2 ± 0.18	–49.8	13.5	
	2-1	1.30	0.049	0.56	8.3 ± 0.3	–49.7	10.4	
GY Per	1-0	2.60	0.020	–	–	–	–	
	2-1	1.30	0.036	–	–	–	–	
UV Aur	1-0	2.60	0.012	–	–	(–14/–24)	–	
	2-1	1.30	0.023	–	–	–	–	
	HCN	3.38	0.010	–	–	–	–	
	SO	1.36	0.050	–	–	–	–	
ZZ Gem	1-0	2.60	0.015	0.07	0.6 ± 0.1	63	–	
	2-1	1.30	0.036	0.21	1.9 ± 0.13	65.5	6.4	
	HCN	3.38	0.012	–	<0.5	–	–	
	SO	1.36	0.057	–	<0.55	–	–	
AFGL 935	1-0	1.63	0.037	0.43	9.5 ± 0.3	25.5	16.7	
	2-1	0.81	0.057	0.84	17.9 ± 0.2	25.4	16.5	
IRAS 06582+1507	1-0	1.63	0.036	0.41	8.7 ± 0.3	21.2	15.7	
	2-1	1.30	0.057	0.67	13.2 ± 0.4	22.0	14.9	
R CMi	1-0	2.60	0.037	–	–	(19/34)	–	
	2-1	1.30	0.076	–	–	–	–	
VX Gem	1-0	2.60	0.036	–	–	(29/48)	–	
	2-1	1.30	0.064	–	–	–	–	
C1698	1-0	2.60	0.042	–	–	(79)	–	
	2-1	1.30	0.086	–	–	–	–	
R Pyx	1-0	2.60	0.030	0.12(:)	2(:)	20(:)	–	
	2-1	1.30	0.038	0.42	5.7 ± 0.2	21.5	8.8	
V CrB	1-0	1.63	0.029	0.61	7.6 ± 0.16	–98.9	8.1	
	2-1	0.81	0.040	1.87	20.0 ± 0.2	–98.7	8.1	
V Oph	1-0	2.60	0.023	0.08(:)	1.0(:)	–28	–	
	2-1	1.30	0.033	0.43	4.4 ± 0.14	–27.2	7.1	
AFGL 2310	1-0	1.63	0.036	0.87	41 ± 1.3	16	25	
	2-1	0.81	0.058	2.83	134 ± 1.3	15.7	27.0	
AFGL 2368	1-0	1.63	0.030	0.56	26.5 ± 0.4	17.1	27.1	
	2-1	0.81	0.057	1.57	70 ± 1	18.2	27.9	
AFGL 2686	1-0	1.63	0.065	0.78	32.1 ± 0.7	0.26	25.6	
	2-1	0.81	0.114	2.27	88.3 ± 0.8	–0.21	24.4	
	HCN	2.11	0.023	0.51	17.8 ± 0.2	2.2	27.5	
	SO	1.36	0.056	–	<4.5	–	–	
V1549 Cyg	1-0	1.63	0.026	0.77	16 ± 0.5	5(:)	17(:)	
	2-1	0.81	0.043	2.41	60 ± 2	5(:)	18.2	
AX Cep	1-0	2.60	0.024	0.36	7.4 ± 0.3	13.3	13.2	
	2-1	1.30	0.031	0.47	8.0 ± 0.6	13.1	13.2	
AFGL 5625	1-0	1.63	0.047	1.57	39.1 ± 0.6	2.3	18.0	
	2-1	0.81	0.064	2.72	64.0 ± 0.6	2.2	18.0	

Table 3. Continued

name	transition	Δv (km s^{-1})	rms (K)	$T_{\rm peak}$ (K)	$\int T$ dv (K km s^{-1})	v$_{\rm c}$ (km s^{-1})	v$_{\rm e}$ (km s^{-1})	remarks
CIT 13	1-0	1.63	0.052	1.24	27.7 ± 0.2	–4.8	13.1	
	2-1	0.81	0.107	2.98	58.5 ± 0.4	–4.2	14.5	
	HCN	2.11	0.024	0.16	3.8 ± 0.4	–2.5	20.9	
	SO	1.36	0.059	–	<2.5	–	–	
AO Lac	1-0	2.60	0.022	–	–	–	–	
	2-1	1.30	0.038	–	–	–	–	
LS Cas	1-0	2.60	0.023	–	–	–	–	
	2-1	1.30	0.038	–	–	–	–	
			O-rich stars					
AFGL 230	1-0	1.63	0.021	0.14(:)	2.2 ± 0.7	–55(:)	14(:)	
	2-1	0.81	0.040	0.72	12.9 ± 0.2	–54.8	13.7	
AFGL 5093	1-0	2.60	0.026	0.08	1.3(:)	–38(:)	12(:)	
	2-1	1.30	0.032	0.26	3.9 ± 0.2	–37.0	11.1	
AFGL 5097	1-0	2.60	0.017	–	<0.7	–	–	
	2-1	2.60	0.013	0.09	1.6 ± 0.1	–54	13.9	
NV Aur	1-0	1.63	0.038	1.03	30.5 ± 0.3	3.3	18.8	
	2-1	0.81	0.072	2.24	60.9 ± 0.4	3.6	18.4	
AFGL 712	1-0	2.60	0.017	0.23	5.0 ±0.13	–31.5	13.6	
	2-1	1.30	0.026	0.25	5.5 ± 0.3	–31.3	13.2	
IRAS 05284+1945	1-0	2.60	0.010	0.07(:)	0.8 ± 0.3	15(:)	15(:)	
	2-1	1.30	0.035	0.12(:)	2.1 ± 0.2	15(:)	15(:)	
IRAS 06403−0138	1-0	2.60	0.015	0.05(:)	0.6(:)	–	–	IS contamination
	2-1	1.30	0.028	0.1(:)	1.4(:)	18	10(:)	
IRAS 07113−2747	1-0	2.60	0.029	0.09	1.8 ± 0.24	96.1	7.6	
	2-1	1.30	0.040	0.24	2.8 ± 0.2	96.0	8.6	
OH 10.1–0.1	1-0	2.60	0.048	–	–	(52.3)	–	
	2-1	1.30	0.052	–	–	–	–	
IRAS 21554+6204	1-0	1.63	0.032	0.82	20.2 ± 0.4	–18.8	18.4	
	2-1	0.81	0.044	1.29	32.0 ± 0.3	–18.8	17.6	
AFGL 2885	1-0	2.60	0.018	0.10	3(:)	–25	17	
	2-1	1.30	0.036	0.45	11.5 ± 0.6	–26.0	17.3	
AFGL 2968	1-0	2.60	0.027	–	<2	–	–	
	2-1	1.30	0.042	0.51	17.7 ± 0.4	–49.3	26.4	
			IRAM January 1995					
			C-stars					
Y Per	1-0	2.60	0.017	0.14	1.4 ± 0.10	–6.7	7.0	
	2-1	1.30	0.031	0.32	3.1 ± 0.14	–7.0	7.4	
	3-2	2.17	0.059	0.16(:)	1.5 ± 0.1	–5(:)	6.8(:)	
R Ori	1-0	2.60	0.016	–	<0.5	–	–	
	2-1	2.60	0.043	0.12(:)	1.4 ± 0.7	15(:)	10(:)	
V Aur	1-0	2.60	0.027	–	<2	–	–	
	2-1	2.60	0.037	0.16	4.1±0.5	0(:)	20(:)	
	3-2	1.08	0.348	–	<15	–	–	
ZZ Gem	1-0	2.60	0.018	–	<0.5	–	–	
	2-1	1.30	0.033	0.22	2.0 ± 0.2	64.9	7.3	
	3-2	1.08	0.094	–	<2	–	–	
R CMi	1-0	2.60	0.028	–	–	–	–	
	2-1	1.30	0.085	–	–	–	–	
R Pyx	1-0	2.60	0.087	–	<2	–	–	
	2-1	1.30	0.106	0.4(:)	4.8 ± 0.5	21.3(:)	8.2	
	3-2	1.08	0.388	–	<10	–	–	
V CrB	1-0	0.81	0.033	0.57	6.92 ± 0.10	–99.3	8.2	
	2-1	1.30	0.048	2.14	23.1 ± 0.3	–98.9	8.7	
	3-2	1.08	0.121	1.36	14.1 ± 0.48	–97.1	7.8	
V Oph	1-0	2.60	0.025	0.1(:)	<1	–	–	
	2-1	1.30	0.072	0.50	5.0 ± 0.3	–27.7	6.9	
AX Cep	1-0	1.63	0.027	0.37	7.83 ± 0.15	12.9	12.1	
	2-1	1.30	0.036	0.91	16.9 ± 0.2	13.3	12.8	
	3-2	2.17	0.064	0.3(:)	4.6 ± 0.6	15(:)	11(:)	

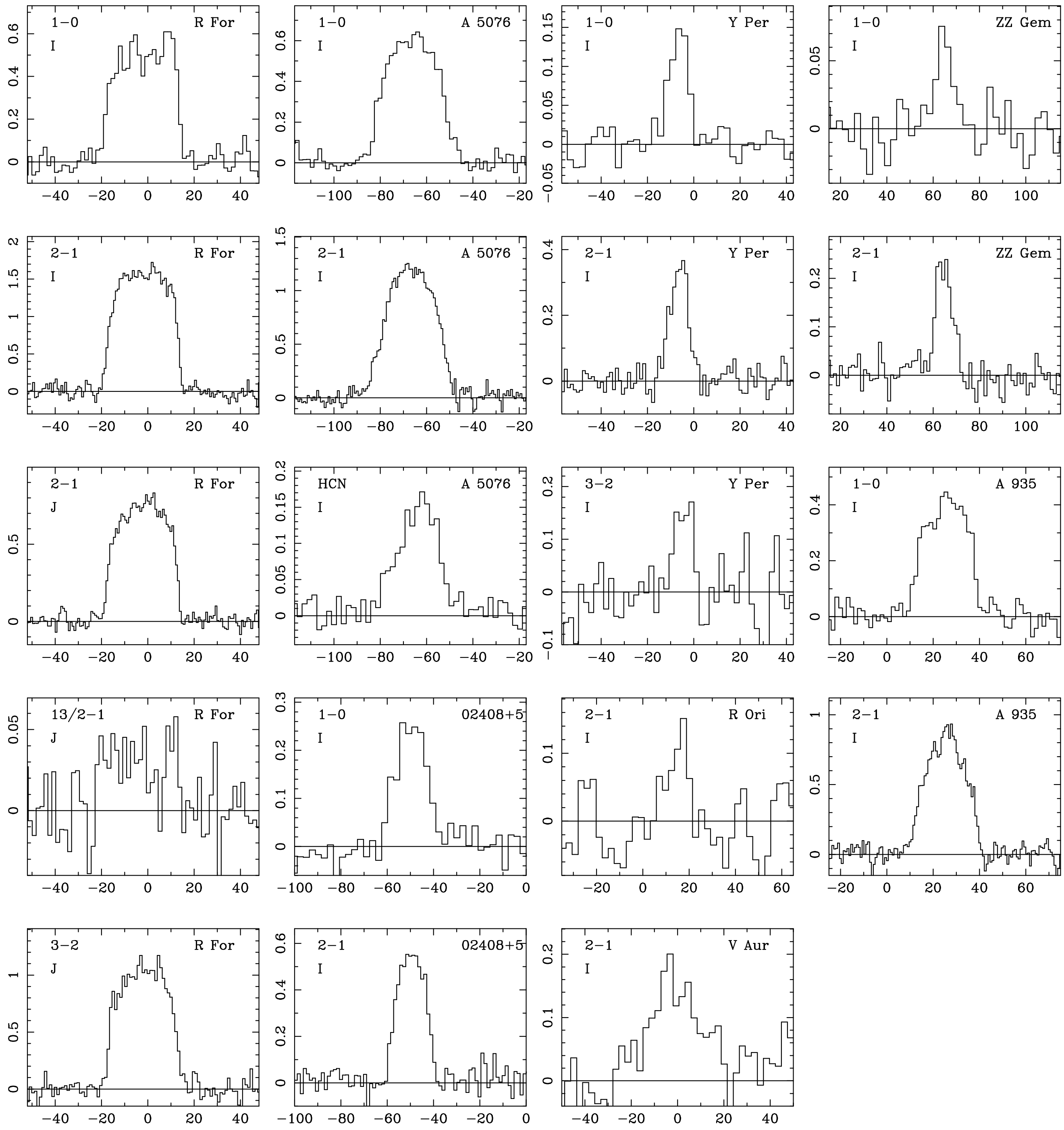

Fig. 1. Line profiles of the carbon stars. Velocity scale is relative to the LSR. Temperatures are on main-beam scale. In the upper left-hand corner the transition, and telescope is indicated: 'I', 'J', 'S', stand for IRAM, JCMT and SEST, respectively.

observations were obtained using a throw of 20″. The observation was obtained on November 28, 1998, and the results are listed in Table 4. For four stars these appear to be the first NIR measurements published, which will be used later on to obtain the distance using a period-$M_{\rm K}$-relation.

5. Analysis

5.1. Modelling some SEDs

A few very red stars without known pulsation period (all observed with the IRAM-30m-telescope in December 1994) are treated in a different way from the rest of the sample. The reason is that for some objects no near-IR data

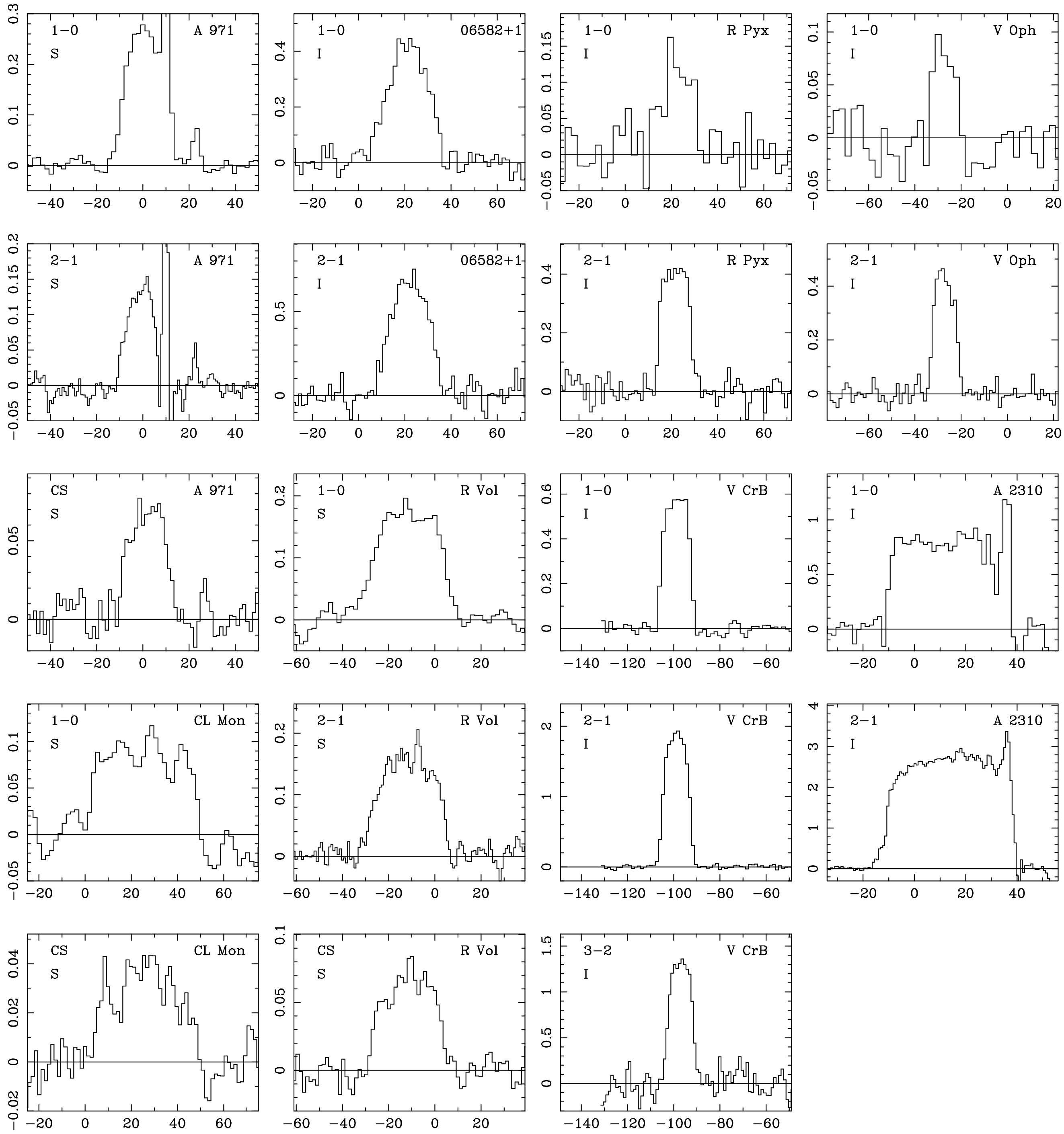

Fig. 2. As Fig. 1.

and/or pulsation period is available and the methods discussed below could not be applied.

The object OH 10.1–0.1 (IRAS 18052–2016) is located near the galactic centre and thus we assume a distance of 8.0 kpc. The other objects (IRAS 02408+5458, 06582+1507, 05284+1945, 06403–0138, 21554+6204, 22480+6002 = AFGL 2968) are all located outside the solar circle, and were studied by Blommaert et al. (1993). Following Blommaert et al. (1993), kinematic distances could be derived for all objects except IRAS 05284+1945, which in the following we assume to be located at 5 kpc, for otherwise its luminosity would be too low to be on the AGB. Jiang et al. (1997) put this object at 9.8 kpc (for their assumed typical AGB luminosity of 8000 $L_{\odot}$).

As a next step the SEDs and LRS spectra were fitted using the dust radiative transfer model of Groenewegen

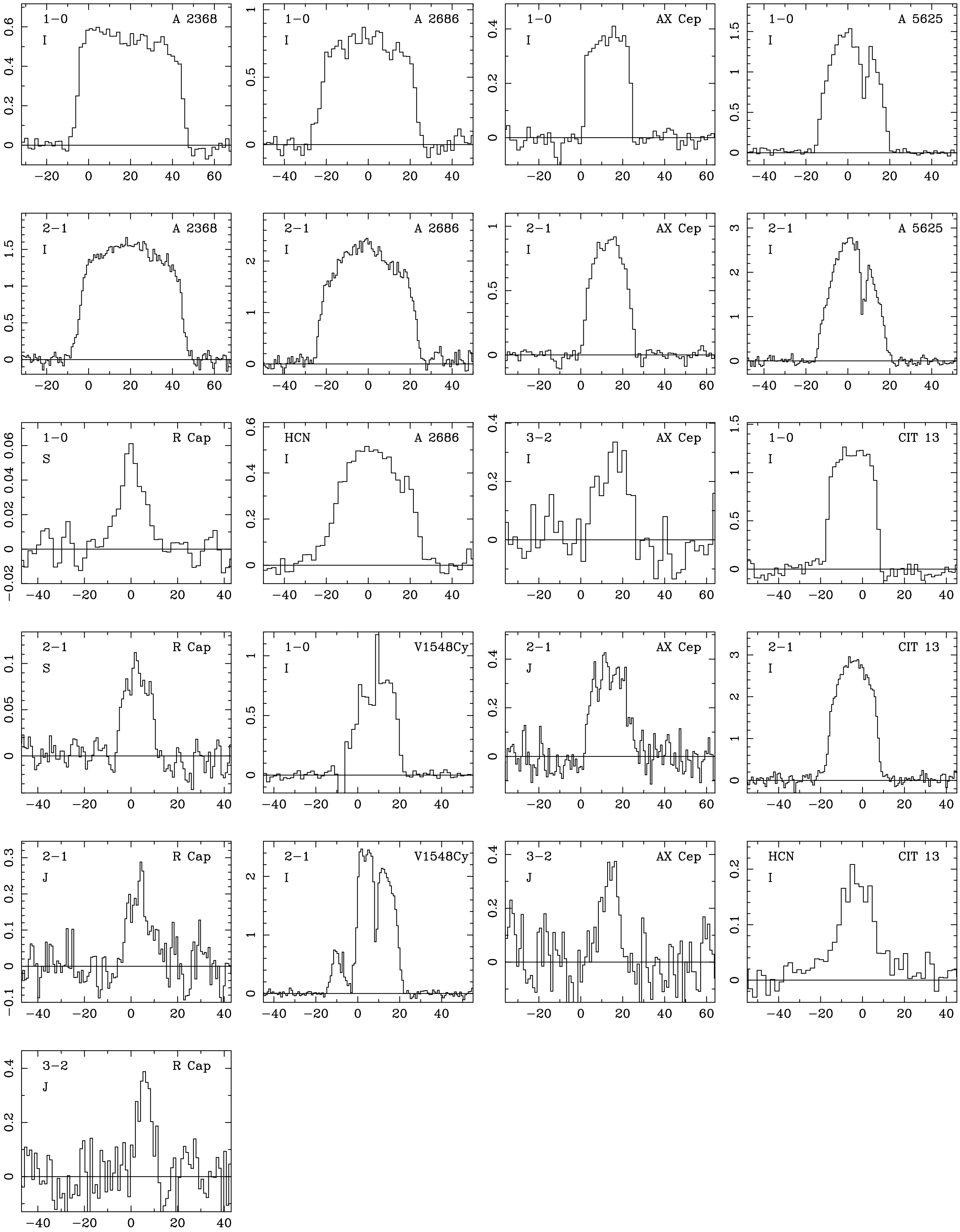
1–0 I A 2368
1–0 I A 2686
1–0 I AX Cep
1–0 I A 5625
2–1 I A 2368
2–1 I A 2686
2–1 I AX Cep
2–1 I A 5625
1–0 S R Cap
HCN I A 2686
3–2 I AX Cep
1–0 I CIT 13
2–1 S R Cap
1–0 I V1548Cy
2–1 J AX Cep
2–1 I CIT 13
2–1 J R Cap
2–1 I V1548Cy
3–2 J AX Cep
HCN I CIT 13
3–2 J R Cap

Fig. 3. As Fig. 1.

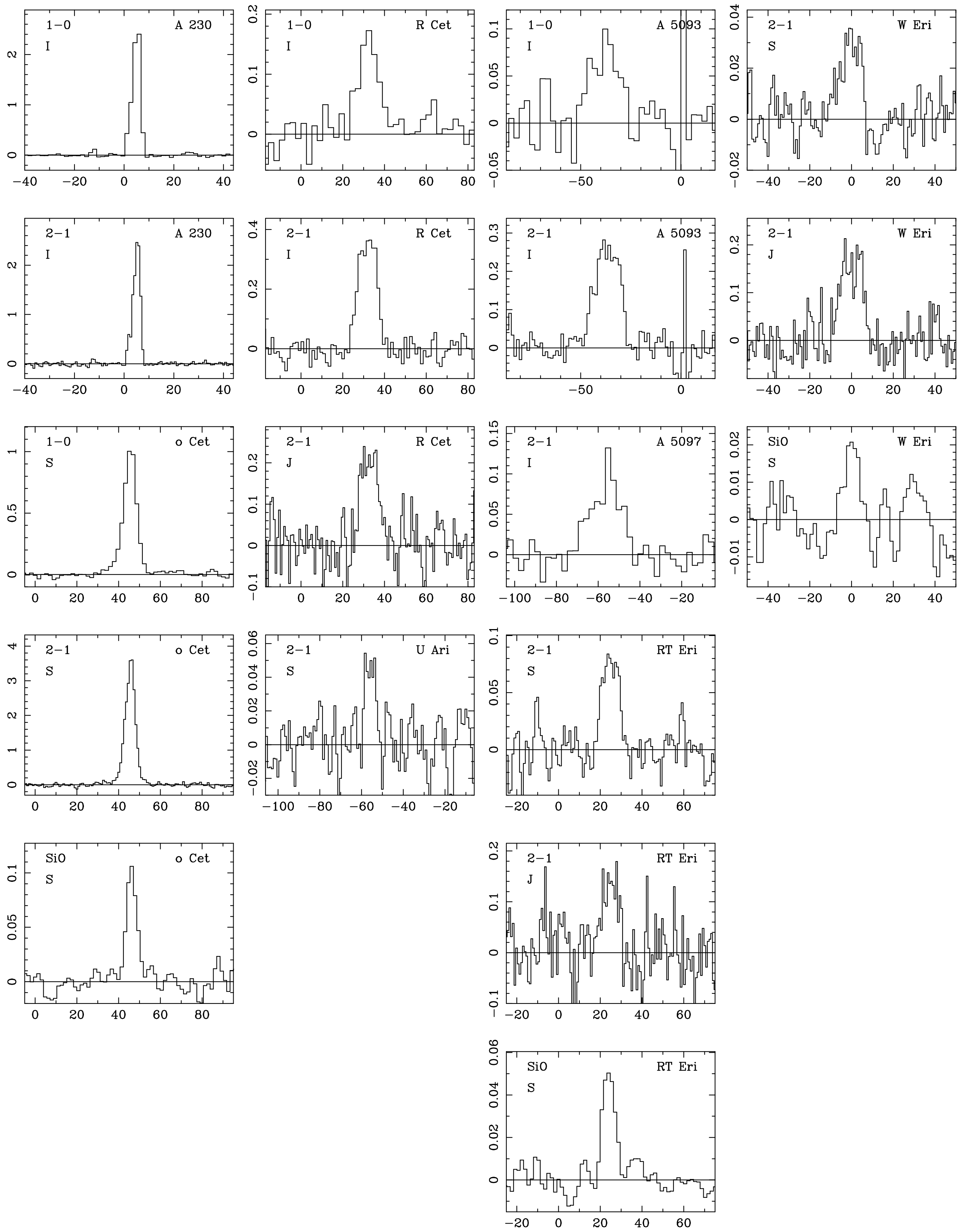

Fig. 4. As Fig. 1, but for the oxygen-rich stars.

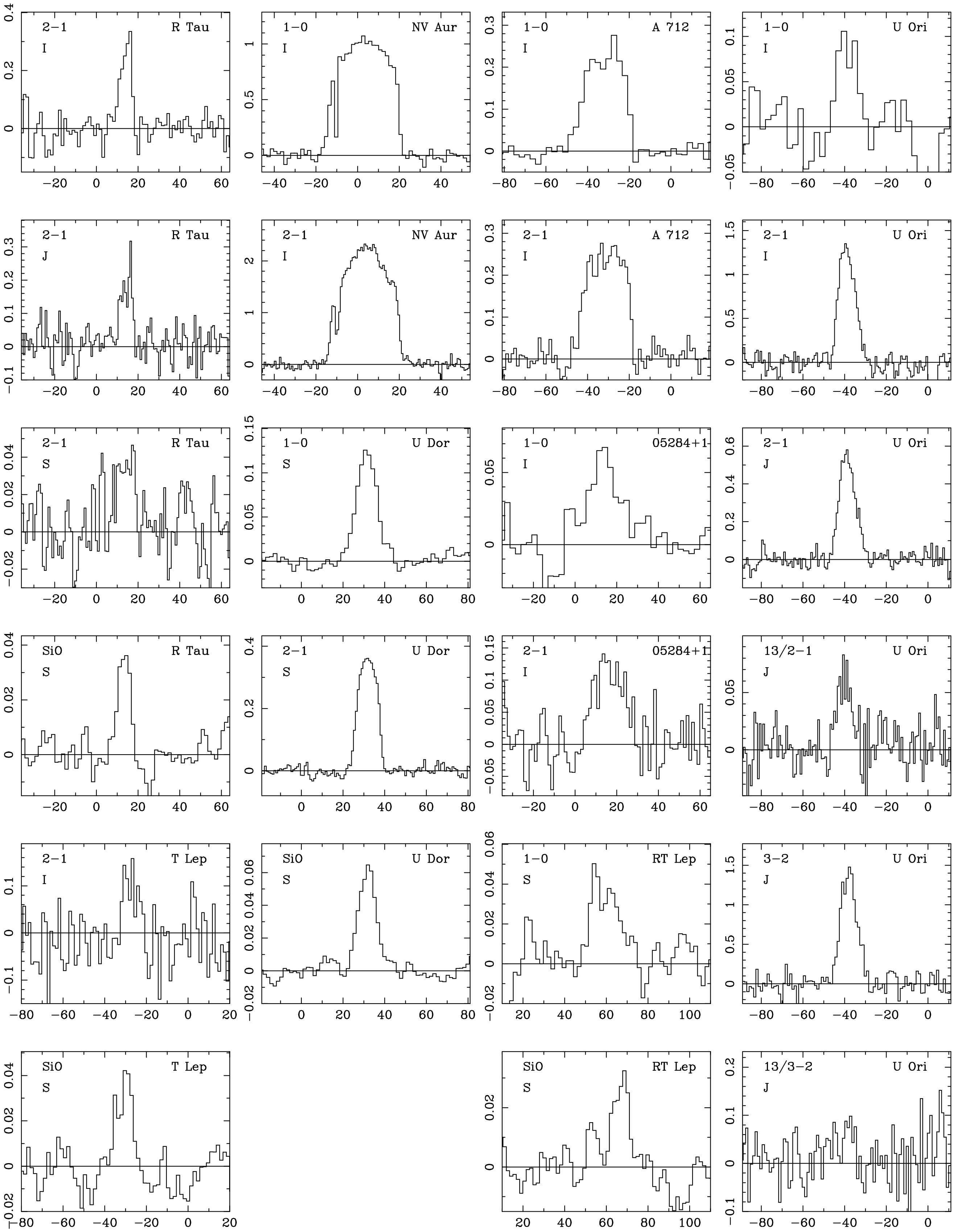

2−1 R Tau I
1−0 NV Aur I
1−0 A 712 I
1−0 U Ori I
2−1 R Tau J
2−1 NV Aur I
2−1 A 712 I
2−1 U Ori I
2−1 R Tau S
1−0 U Dor S
1−0 05284+1 I
2−1 U Ori J
SiO R Tau S
2−1 U Dor S
2−1 05284+1 I
13/2−1 U Ori J
2−1 T Lep I
SiO U Dor S
1−0 RT Lep S
3−2 U Ori J
SiO T Lep S
SiO RT Lep S
13/3−2 U Ori J

Fig. 5. As Fig. 4.

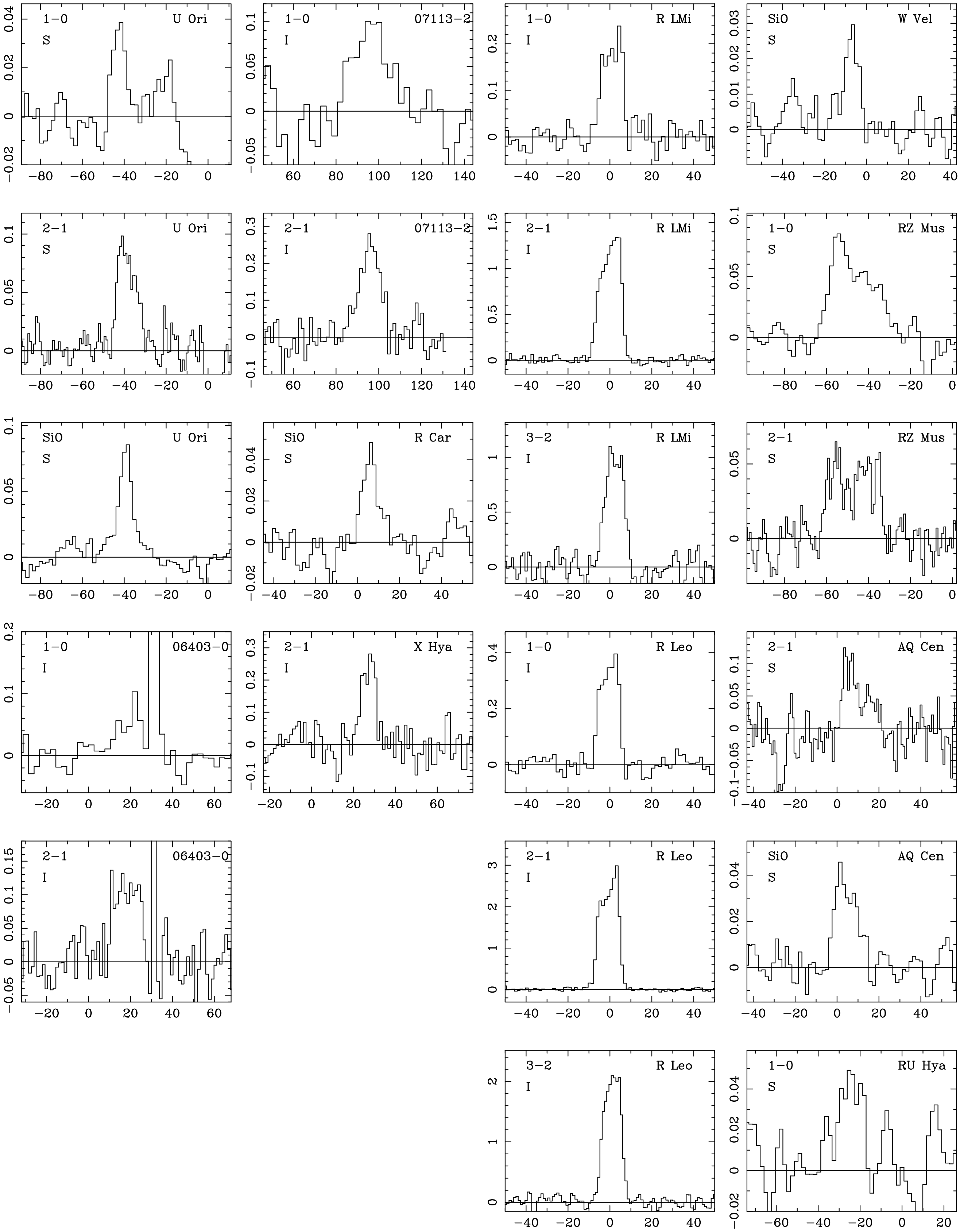
1−0 U Ori S
1−0 07113−2 I
1−0 R LMi I
SiO W Vel S
2−1 U Ori S
2−1 07113−2 I
2−1 R LMi I
1−0 RZ Mus S
SiO U Ori S
SiO R Car S
3−2 R LMi I
2−1 RZ Mus S
1−0 06403−0 I
2−1 X Hya I
1−0 R Leo I
2−1 AQ Cen S
2−1 06403−0 I
2−1 R Leo I
SiO AQ Cen S
3−2 R Leo I
1−0 RU Hya S

Fig. 6. As Fig. 4.

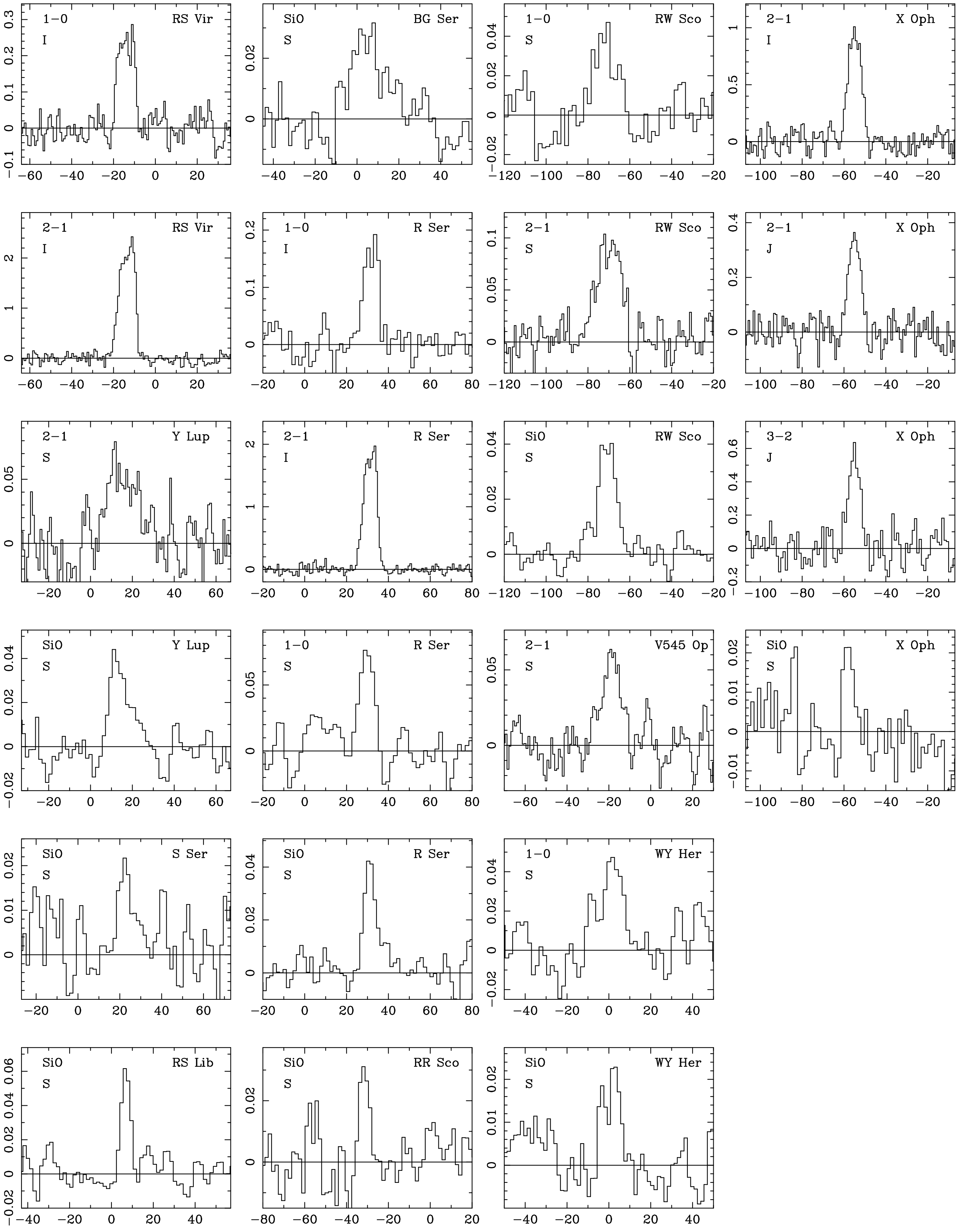
1−0 I RS Vir
SiO S BG Ser
1−0 S RW Sco
2−1 I X Oph
2−1 I RS Vir
1−0 I R Ser
2−1 S RW Sco
2−1 J X Oph
2−1 S Y Lup
2−1 I R Ser
SiO S RW Sco
3−2 J X Oph
SiO S Y Lup
1−0 S R Ser
2−1 S V545 Op
SiO S X Oph
SiO S S Ser
SiO S R Ser
1−0 S WY Her
SiO S RS Lib
SiO S RR Sco
SiO S WY Her

Fig. 7. As Fig. 4.

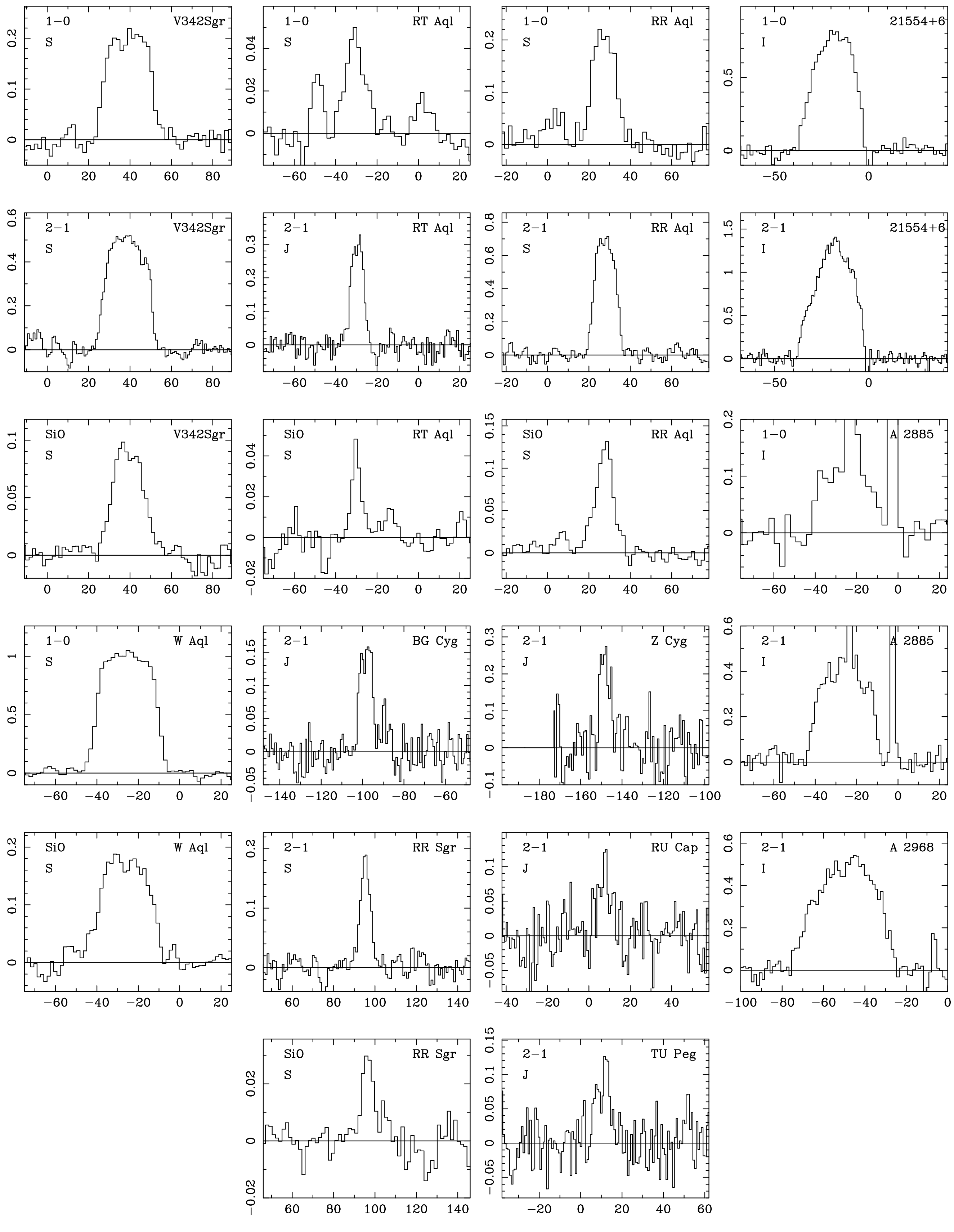
1−0 V342Sgr S
1−0 RT Aql S
1−0 RR Aql S
1−0 21554+6 I
2−1 V342Sgr S
2−1 RT Aql J
2−1 RR Aql S
2−1 21554+6 I
SiO V342Sgr S
SiO RT Aql S
SiO RR Aql S
1−0 A 2885 I
1−0 W Aql S
2−1 BG Cyg J
2−1 Z Cyg J
2−1 A 2885 I
SiO W Aql S
2−1 RR Sgr S
2−1 RU Cap J
2−1 A 2968 I
SiO RR Sgr S
2−1 TU Peg J

Fig. 8. As Fig. 4.

Table 3. Continued

name	transition	Δv (km s^{-1})	rms (K)	$T_{\rm peak}$ (K)	$\int T$ dv (K km s^{-1})	v$_{\rm c}$ (km s^{-1})	v$_{\rm e}$ (km s^{-1})	remarks
			O-rich stars					
U Ori	1-0	2.60	0.028	0.1(:)	1.2(:)	–40(:)	7(:)	
	2-1	0.81	0.089	1.26	12.3 ± 0.8	–38.5	8.0	
R LMi	1-0	1.63	0.023	0.18	2.26 ± 0.10	0.94	7.2	
	2-1	1.30	0.034	1.25	14.9 ± 0.17	0.04	8.6	
	3-2	1.08	0.099	1.03	10.9 ± 0.5	2.2	8.2	
R Leo	1-0	1.63	0.026	0.34	3.87 ± 0.13	–0.58	7.2	
	2-1	1.30	0.033	2.6(:)	28.6 ± 0.3	–0.63	7.2	
	3-2	1.08	0.075	2.07	19.8 ± 0.4	1.1	7.5	
RS Vir	1-0	0.81	0.038	0.24	2.31 ± 0.10	–14.0	5.7	
	2-1	0.81	0.092	2.25	19.5 ± 0.3	–13.5	6.7	
R Ser	1-0	1.63	0.024	0.16	1.37 ± 0.10	31.6	5.3(:)	
	2-1	0.81	0.059	1.84	13.2 ± 0.3	31.3	6.4	
X Oph	1-0	1.63	0.038	–	<0.8	–	–	
	2-1	0.81	0.079	0.93	7.3 ± 0.3	–54.9	6.3	
R Peg	1-0	1.63	0.027	0.08(:)	0.7± 0.1	25.5(:)	7.3(:)	
	2-1	1.30	0.025	0.68	5.77 ± 0.10	24.4	6.0	
	3-2	1.08	0.065	0.64	5.2 ± 0.2	25.6	6.6	
			IRAM August 1995 run					
			O-rich stars					
R Cet	1-0	2.60	0.025	0.15	1.8 ± 0.1	32.2	9.9	
	2-1	1.30	0.035	0.37	3.9 ± 0.1	31.9	8.6	
R Tri	1-0	2.60	0.016	–	–	(56/64)	–	
	2-1	1.30	0.026	–	–	–	–	
R Tau	1-0	2.60	0.023	–	–	–	–	
	2-1	1.30	0.043	0.26	1.8 ± 0.1	14.1	5.6	
T Lep	1-0	2.60	0.037	–	–	–	–	
	2-1	1.30	0.055	0.1 (:)	0.6 (:)	–27 (:)	6.8 (:)	
X Hya	1-0	2.60	0.049	–	–	–	–	
	2-1	1.30	0.053	0.23	1.9 ± 0.2	27.0	6.8	
R Aqr	1-0	2.60	0.027	–	–	–	–	
	2-1	1.30	0.033	0.073	1.5 ± 0.2	–30.4	16.7	
			IRAM combined December 1994 & January 1995 run					
ZZ Gem	2-1	1.30	0.026	0.24	2.1 ± 0.1	65.0	6.9	
R CMi	1-0	2.60	0.022	–	–	–	–	
	2-1	1.30	0.057	–	–	–	–	
V CrB	1-0	1.63	0.019	0.59	7.2 ± 0.1	–98.9	8.2	
	2-1	1.30	0.025	1.91	21.9 ± 0.2	–98.9	8.3	
V Oph	1-0	2.60	0.018	0.1	0.7(:)	–27.6	8(:)	
	2-1	1.30	0.032	0.44	4.7 ± 0.1	–27.3	7.8	

(1993; also see Groenewegen et al. 1998). IRAS LRS spectra could be retrieved from the database maintained at the University of Calgary (see

http://www.iras.ucalgary.ca/~volk/getlrs_plot.html), except for IRAS 05284+1945. Broadband data were taken from the IRAS Point Source Catalog (12, 25, 60, 100 μm data), and IR data from Blommaert et al. (1993)(typically $JHKLM$ and narrow-band data near 10 μm in the best cases, but note that *no* near-IR data is available for IRAS 18052–2016 and 21554+6204). For IRAS 05284+1945 a K observation was taken from from Garcia-Lario et al. (1997) and H, K observations from Jiang et al. (1997). For AFGL 2968, I, K observations were added from the IRC survey.

The interstellar extinction towards the sources was estimated from the model by Arenou et al. (1992), and ranges from $A_{\rm V}$ = 0.5 - 3.0. For OH 10.1–0.1, probably a Galactic Center source, we assumed an $A_{\rm V}$ of 25. Within the uncertainties, in none of the cases does the adopted value for the extinction influence the derived value for luminosity or dust mass loss rate. The model requires the expansion velocity of the outflow which is taken from the CO measurements.

Table 3. Continued

name	transition	Δv (km s^{-1})	rms (K)	$T_{\rm peak}$ (K)	$\int T$ dv (K km s^{-1})	v$_{\rm c}$ (km s^{-1})	v$_{\rm e}$ (km s^{-1})	remarks
			JCMT August 1995 run					
			C-stars					
R For	12/2-1	0.81	0.036	0.8	20.6	−2.1	17.8	
	13/2-1	1.70	0.019	–	1.1(:)	–	–	
	12/3-2	1.08	0.082	1.2	28.5	−2.0	19.0	
UV Aur	2-1	0.81	0.048	–	–	–	–	
R Cap	2-1	0.81	0.046	0.25	2.52	2.6	10.5	
	3-2	1.08	0.083	0.35	2.4	5.6	8(:)	
AX Cep	2-1	0.81	0.060	0.40	6.5	13.1	13.0	
	3-2	1.08	0.109	0.35	2.2	15.1	–	
			O-rich stars					
S Scl	2-1	0.81	0.064	–	–	(8.5)	–	
R Cet	2-1	0.81	0.053	0.2	2.1	32.1	7.5	
RT Eri	2-1	0.81	0.054	0.15	1.4	24.7	8.5	
W Eri	2-1	0.81	0.040	0.18	1.9	0.2	10.0	
RS Eri	2-1	0.81	0.055	–	–	(49)	–	
R Tau	2-1	0.81	0.050	0.2	1.4	14.6	5.0	
BD Eri	2-1	0.81	0.051	–	–	(−11)	–	
T Lep	2-1	0.81	0.058	–	–	–	–	
U Ori	12/2-1	0.81	0.033	0.6	5.2	−38.6	9.7	
	13/2-1	0.85	0.019	0.06(:)	0.49(:)	−40.5	–	
	12/3-2	1.08	0.102	1.5	13.5	−37.8	9.2	
	13/3-2	1.13	0.057	0.06(:)	0.7(:)	–	–	
X Oph	2-1	0.81	0.051	0.35	2.12	−55.0	6.3	
	3-2	1.08	0.091	0.60	3.77	−54.9	6.5	
RT Aql	2-1	0.81	0.026	0.32	2.1	−29.5	6.5	
BG Cyg	2-1	0.81	0.021	0.15	1.4	−97.6	5.0	
Z Cyg	2-1	0.81	0.054	0.26	1.8	−148.4	4.5	
RU Cap	2-1	0.81	0.031	0.1(:)	0.7(:)	7.5(:)	7.5(:)	
TU Peg	2-1	0.81	0.030	0.1(:)	0.9	12.4	8.0(:)	
R Peg	2-1	0.81	0.036	0.24	2.0	24.3	6.5	
	3-2	1.08	0.175	0.4(:)	4.0(:)	16.5	–	
W Peg	2-1	0.81	0.027	0.3	3.6	−14.8	8.1	
	3-2	1.08	0.109	0.6	4.8	−16.4	8.1	
R Aqr	2-1	0.81	0.054	–	–	–	–	

Table 2. Lines observed

Line	Frequency (MHz)	Teles.	F$_{\rm eff}$	B$_{\rm eff}$	Beam ($''$)
^{12}CO(1-0)	115271.204	IRAM	0.92	0.67	20.9
		SEST		0.70	45
^{13}CO(2-1)	220396.700	JCMT		0.69	22.0
^{12}CO(2-1)	230537.990	IRAM	0.86	0.39	10.4
		JCMT		0.69	21.1
		SEST		0.60	23
^{13}CO(3-2)	330587.959	JCMT		0.58	14.7
^{12}CO(3-2)	345795.975	IRAM	0.77	0.25	8.3
		JCMT		0.58	14.1
HCN(1-0)	88631.602	IRAM	0.92	0.76	27.0
SiO (3-2,v=0)	130268.702	SEST		0.69	42
CS (3-2)	146969.047	SEST		0.67	34
SO(6_5-5_4)	219949.391	IRAM	0.86	0.41	10.9

The resulting fits are displayed in Figs. 10-16. We find two sources to be carbon-rich: IRAS 02408+5458 and 06582+1507. This was already suggested by Blommaert et al. (1993) based on the shape of the SEDs, and by Volk et al. (1993) based on the characteristic featureless LRS spectra of very red carbon stars (see also the group V sources in Groenewegen et al. 1992). This is indirectly confirmed here by the good fits obtained with amorphous carbon dust. Both stars lose mass at such high rates that any presence of silicate would result in deep silicate absorption near 10 μm, which is not observed. The fit to the blue part of the LRS spectrum of IRAS 02408+5458 is not very good however. Recently, Speck et al. (1997) obtained an UKIRT CGS3 8-13 μm spectrum. Their spectrum differs in two ways from the LRS spectrum. First, their spectrum continues to rise to the blue, peaks near 9 μm and only then drops in flux towards shorter wavelengths, in much better agreement with our model prediction. Second, they find strong silicon carbide absorption at 11 μm, which is not evident in the LRS spectrum. To simulate this, our model was calculated with 90% amorphous car-

Table 3. Continued

name	transition	Δv (km s^{-1})	rms (K)	$T_{\rm peak}$ (K)	$\int T$ dv (K km s^{-1})	v$_c$ (km s^{-1})	v$_e$ (km s^{-1})	remarks
			SEST combined runs					
			C-stars					
AFGL 971	1-0	1.80	0.015	0.27	6.0	0.8	13.5	
	2-1	0.91	0.012	0.14	2.4	−1.0	10.4(:)	
	CS	1.42	0.011	0.070	1.3	1.2	13.3	
CL Mon	1-0	1.80	0.019	0.10	3.6	25.3	24.5	
	CS	1.42	0.009	0.04	1.3	25.8	23.8	
R CMi	1-0	1.80	0.017	–	–	–	–	
	CS	1.42	0.010	–	–	–	–	
R Vol	1-0	1.80	0.015	0.18	5.6	−11.8	22.1	
	2-1	0.91	0.012	0.16	4.6	−11.7	18.8	
	CS	1.42	0.009	0.070	1.9	−11.4	17.9	
R Pyx	1-0	1.80	0.015	–	–	–	–	
	CS	1.42	0.010	–	–	–	-	
V Cru	1-0	1.80	0.015	–	–	–	–	
	CS	1.42	0.010	–	–	–	–	
R Cap	1-0	1.80	0.007	0.060	0.66	0.2	11.0(:)	
	2-1	0.91	0.013	0.090	1.2	2.6	8.9	
	CS	1.42	0.008	–	–	–	–	
	SiO	1.60	0.006	–	–	–	–	
RZ Peg	1-0	1.80	0.023	–	–	(–15/–34)	–	
	2-1	0.91	0.029	–	–	–	–	
	CS	1.42	0.011	–	–	–	–	
			O-rich stars					
o Cet	1-0	1.80	0.018	1.0	8.0	45.2	19.1	
	2-1	0.91	0.043	3.6	21.6	45.4	15.7	
	SiO	1.60	0.009	0.10	0.73	46.3	15.9	
U Ari	1-0	1.80	0.014					
	2-1	0.91	0.014	0.047	0.30	−56.2	4.4	
	SiO	1.60	0.008					
RT Eri	1-0	1.80	0.011					
	2-1	0.91	0.017	0.081	0.73	24.7	6.9	
	SiO	1.60	0.006	0.050	0.40	24.3	5.8	
U Hor	1-0	1.80	0.011	–	–	(–35)	–	
	SiO	1.60	0.008	–	–	–	–	
W Eri	1-0	1.80	0.007	–	–	–	–	
	2-1	0.91	0.008	0.032	0.34	0.6	8.8(:)	
	SiO	1.60	0.006	0.020	0.10	0.0	7.1	
R Tau	1-0	1.80	0.011	–	–	–	–	
	2-1	0.91	0.014	0.039	0.40	12.9	5.9(:)	
	SiO	1.60	0.006	0.035	0.25	13.5	5.6	
RX Tau	1-0	1.80	0.011	–	–	(–36)	–	
	2-1	0.91	0.010	–	–	–	–	
	SiO	1.60	0.010	–	–	–	–	
R Cae	1-0	1.80	0.018	–	–	(3)	–	
	SiO	1.60	0.009	–	–	–	–	
T Lep	1-0	1.80	0.012	–	–	–	–	
	2-1	0.91	0.017	–	–	–	–	
	SiO	1.60	0.008	0.039	0.23	−30.2	7.3	
U Dor	1-0	1.80	0.008	0.12	1.5	31.2	11.0	
	2-1	0.91	0.013	0.36	3.9	31.8	8.4	
	SiO	1.60	0.005	0.064	0.64	31.4	9.8	
RT Lep	1-0	1.80	0.013	0.04	0.63	55.0	11.9(:)	
	SiO	1.60	0.007	0.03	0.34	68.	–	
U Ori	1-0	1.80	0.010	0.04	–	−41.	7.4	
	2-1	0.91	0.010	0.097	1.2	−38.7	7.6	
	SiO	1.60	0.007	0.084	0.72	−39.2	7.6	

Table 3. Continued

name	transition	Δv (km s^{-1})	rms (K)	$T_{\rm peak}$ (K)	$\int T$ dv (K km s^{-1})	v$_{\rm c}$ (km s^{-1})	v$_{\rm e}$ (km s^{-1})	remarks
AS Pup	1-0	1.80	0.015	–	–	(–33)	–	
	SiO	1.60	0.008	–	–	–	–	
R Car	1-0	1.80	0.013	–	–	–	–	
	2-1	0.91	0.017	–	–	–	–	
	SiO	1.60	0.008	0.047	0.40	5.2	6.8(:)	
W Vel	1-0	1.80	0.010	–	–	–	–	IS contamination
	2-1	0.91	0.016	–	–	–	–	IS contamination
	SiO	1.60	0.005	0.029	0.24	−6.5	6.4	
RZ Mus	1-0	1.80	0.009	0.080	1.64	−47.5	18.9	
	2-1	0.91	0.014	0.054	1.14	−45.5	15.5	
	SiO	1.60	0.006	–	–	–	–	
AQ Cen	1-0	1.80	0.016	–	–	–	–	
	2-1	0.91	0.036	0.11	1.0	9.1	10.2	
	SiO	1.60	0.008	0.043	0.49	5.0	9.5	
RU Hya	1-0	1.80	0.015	0.048	0.65	−24.2	7.4(:)	
	SiO	1.60	0.008	–	–	–	–	
Y Lup	1-0	1.80	0.014	–	–	–	–	
	2-1	0.91	0.021	0.053	0.97	17.1	13.8	
	SiO	1.60	0.008	0.040	0.32	17.6	11.3	
S Ser	1-0	1.80	0.017	–	–	–	–	
	SiO	1.60	0.008	0.021	0.20	23.4	8.8(:)	
RS Lib	1-0	1.80	0.015	–	–	–	–	
	SiO	1.60	0.008	0.060	0.31	7.0	4.5	
BG Ser	1-0	1.80	0.015	–	–	–	–	
	SiO	1.60	0.009	0.029	0.53	5.5	11(:)	
R Ser	1-0	1.80	0.015	0.073	0.57	29.7	6.6	
	SiO	1.60	0.007	0.041	0.35	31.8	6.1	
RR Sco	1-0	1.80	0.012	–	–	–	–	
	2-1	0.91	0.018	–	–	–	–	
	SiO	1.60	0.008	0.031	0.12	−31.3	5.3	
RW Sco	1-0	1.80	0.011	0.043	0.48	−70.3	11.0	
	2-1	0.91	0.016	0.094	1.30	−70.7	10.5	
	SiO	1.60	0.004	0.037	0.44	−70.7	10.6	
V545 Oph	1-0	1.80	0.011	–	–	–	–	
	2-1	0.91	0.011	0.060	0.63	−18.7	9.3	
	SiO	1.60	0.009	–	–	–	–	
V438 Sco	1-0	1.80	0.015	–	–	–	–	
	2-1	0.91	0.018	–	–	–	–	
	SiO	1.60	0.011	–	–	–	–	
WY Her	1-0	1.80	0.013	0.045	0.62	0.3	11.7	
	SiO	1.60	0.006	0.022	0.15	1.8	9.0	
X Oph	1-0	1.80	0.012	–	–	–	–	
	2-1	1.82	0.015	–	–	–	–	
	SiO	1.60	0.008	0.020	0.1	−57.6	5.5(:)	
V342 Sgr	1-0	1.80	0.018	0.20	4.9	39.2	16.1	
	2-1	0.91	0.036	0.51	11.3	38.4	15.2	
	SiO	1.60	0.007	0.095	1.7	39.9	15.2	
W Aql	1-0	1.80	0.036	1.0	30.5	−25.4	20.7	
	SiO	1.60	0.014	0.18	4.9	−26.5	17.9	
RT Aql	1-0	1.80	0.010	0.047	0.53	−30.8	9.5(:)	
	SiO	1.60	0.006	0.047	0.26	−30.2	6.5	
RR Sgr	1-0	1.80	0.012		–	–	–	
	2-1	0.91	0.018	0.18	1.2	95.3	5.2	
	SiO	1.60	0.006	0.029	0.24	96.0	5.6	
RR Aql	1-0	1.80	0.020	0.21	2.9	27.1	10.0	
	2-1	0.91	0.031	0.69	8.2	27.9	8.7	
	SiO	1.60	0.008	0.13	1.33	27.3	10.2	

Table 4. NIR photometry

Name	J	H	K
V390 Cas	6.51 ± 0.02	5.22 ± 0.03	4.49 ± 0.02
PT Cas	6.85 ± 0.02	5.74 ± 0.03	5.09 ± 0.02
AFGL 5076	13.9 ± 0.3	13.4 ± 0.1	9.45 ± 0.03
Y Per	4.63 ± 0.02	3.68 ± 0.03	3.25 ± 0.02
GY Per	6.39 ± 0.02	5.32 ± 0.03	4.52 ± 0.02
C1698	7.66 ± 0.02	6.51 ± 0.03	5.78 ± 0.02
U Ari	2.08 ± 0.02	1.20 ± 0.03	0.78 ± 0.02

bon mixed with 10% silicon carbide. The optical depth at 11.3 μm in our model is 5.5. The differences between UKIRT and LRS spectrum may in part be due to the relatively poor signal-to-noise of the LRS spectrum, but the change from a nearly featureless spectrum to one with strong SiC absorption is real, and suggests an increase in the SiC/amorphous carbon ratio.

Applying the adopted kinematic distances and assuming a dust-to-gas ratio of 0.005, we derive for IRAS 02408 +5458 a luminosity of 5700 L$_\odot$ and a mass loss rates of 6.9 $\times$ 10^{-5} M$_\odot$ yr^{-1} and for IRAS 06582+1507 a luminosity of 6500 L$_\odot$ and a mass loss rate of 9.0 $\times$ 10^{-5} M$_\odot$ yr^{-1}. Note that luminosity and mass loss rate scale with the adopted distance like $L \sim D^2$, and $\dot{M} \sim D$.

The other sources are O-rich, as evidenced by the strong silicate emission or absorption. IRAS 05284+1945, for which no LRS spectrum is available, is an OH (te Lintel Hekkert et al. 1991) and SiO (Jiang et al. 1996) maser source. In all stars except one, a silicate dust opacity was used composed of Jones & Merrill (1976) dirty silicate shortward of 8 μm, and the silicate of David & Papoular (1990) at longer wavelengths. The exception is IRAS 18052–2016 (OH 10.1–0.1) where, based on the discussion in Suh (1999), we used $Mg_{0.8}Fe_{0.2}SiO_4$ (Dorschner et al. 1995). This was the only silicate out of several species tried which resulted in at least *some* absorption in the 18 μm region. However, in view of the still not satisfactory fit of the model to the data, further NIR data is badly needed for this source to confirm if the model prediction for the assumed dust opacity holds at shorter wavelengths. The fits to the SEDs and LRS spectra are quite good, the exception being AFGL 2968 (IRAS 22480+6002). However, taking the kinematic distance, we derive a luminosity of 140 000 L$_\odot$, which would make it a supergiant and not an AGB star. In support, its large expansion velocity of 26.4 km s^{-1} and large 60 μm flux to $T(1-0)$ ratio (Josselin et al. 1998) are consistent with this interpretation. In fact, Josselin et al. classified it as a M0I object based on unpublished material (Josselin et al., in preparation). This star has *not* been detected in OH. This is surprising as it is both an SiO (Nyman et al. 1998) and a H_2O master source (Han et al. 1998). Possibly the silicate dust opacity around supergiants is different from that typical for O-rich AGB stars, or the dust is more distributed in a disk-like structure. For the other O-sources we find luminosities in the range 1120 to 30 000 L$_\odot$, and mass loss rates between 5.0 $\times$ 10^{-6} and 6.2 $\times$ 10^{-5} M$_\odot$ yr^{-1}, again assuming a dust-to-gas ratio of 0.005. The luminosity for IRAS 06403–0138 is quite low (1120 L$_\odot$), which might indicate that the kinematic distance is an underestimate of the true distance. Note, again, that luminosity and mass loss rate scale with the adopted distance like $L \sim D^2$, and $\dot{M} \sim D$.

5.2. Luminosity and distance

Luminosities and distances are derived in various ways depending on the amount of available data.

For stars with a pulsation period the luminosity can be derived from a Period-Luminosity (PL) relation. For carbon Miras we use the relation by Groenewegen & Whitelock (1996), which was derived for stars with periods <520 days. This method was used for all carbon stars in the sample, except the five stars with unknown periods. The SEDs of AFGL 5076 and 5625 were fitted by Groenewegen (1995), who assumed a luminosity of 7050 L$_\odot$. This is the mean observed for C-stars in the LMC (see e.g. Groenewegen 1999). In the cases of IRAS 02408+5458 and 06582+1507 we refer to the previous section. C1698 is not considered any further as no sensible assumption for its luminosity and distance can be done.

For oxygen-rich Miras we use the PL-relation by Feast et al. (1989) for LMC Miras shifted by the assumed distance modulus of 18.5 (consistent with the procedure in Groenewegen & Whitelock 1996). This was used for 49 out of the 64 O-rich stars in the sample. For the rest of the sample the luminosity was determined by model fitting the SED (AFGL 5093 in Groenewegen et al. 1995, and the objects discussed in Sect. 5.1), or direct integration under the SED (6 stars; Blommaert et al. 1993), with distance estimates either from kinematics (Blommaert et al. 1994), or the 'phase-lag' method (van Langevelde et al. 1990). The distance and luminosity of the S-star W Aql is discussed in Groenewegen & de Jong (1998) based on a comparison with S-stars in the HIPPARCOS catalog.

The SEDs of 25 out of the 35 C-stars were fitted in Groenewegen et al. (1998), two more in Groenewegen (1995), and two in Sect. 5.1 to give the distance for the adopted luminosity. For three stars, we use the Period-$M_{\rm K}$ relation by Groenewegen & Whitelock (1996), together with the

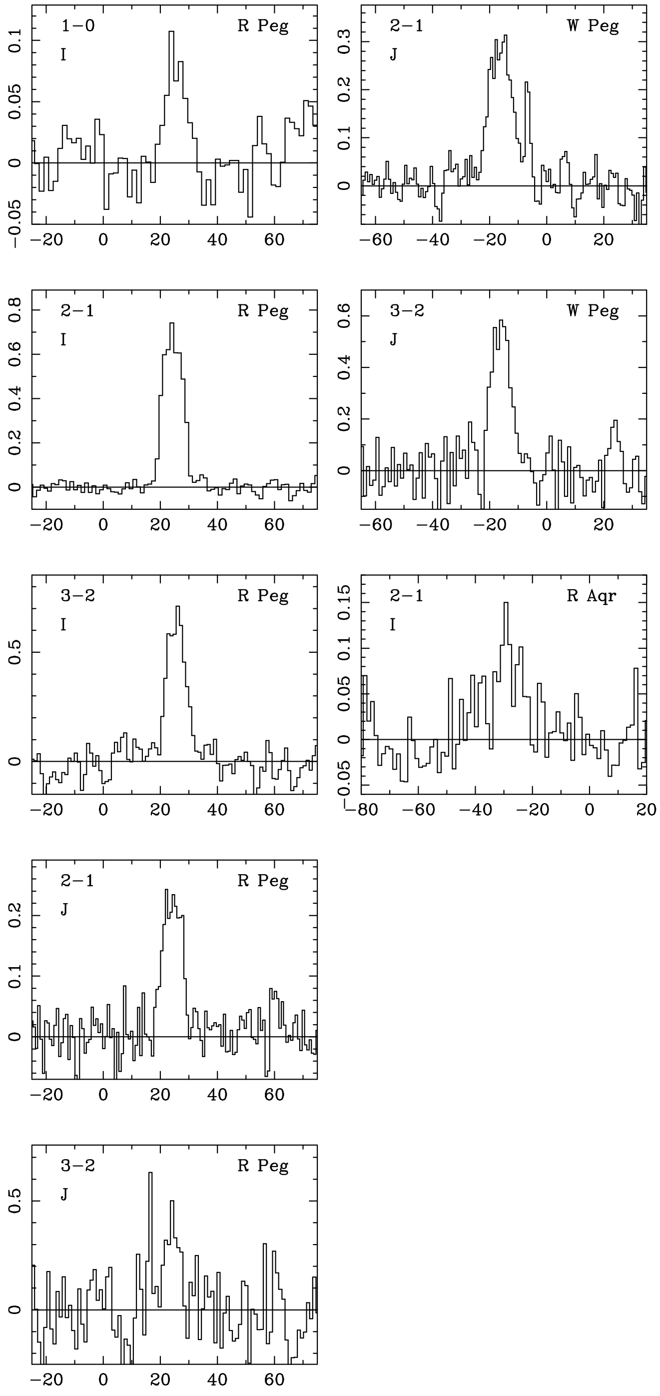

Fig. 9. As Fig. 4.

observed K magnitudes in Table 4, to derive the distance. For three stars no distance could be derived.

As explained above, for some of the O-rich stars there is a kinematic distance or one from the 'phase-lag' method. For some stars distances were derived by Whitelock et al. (1995) based on a method similar to the one described now.

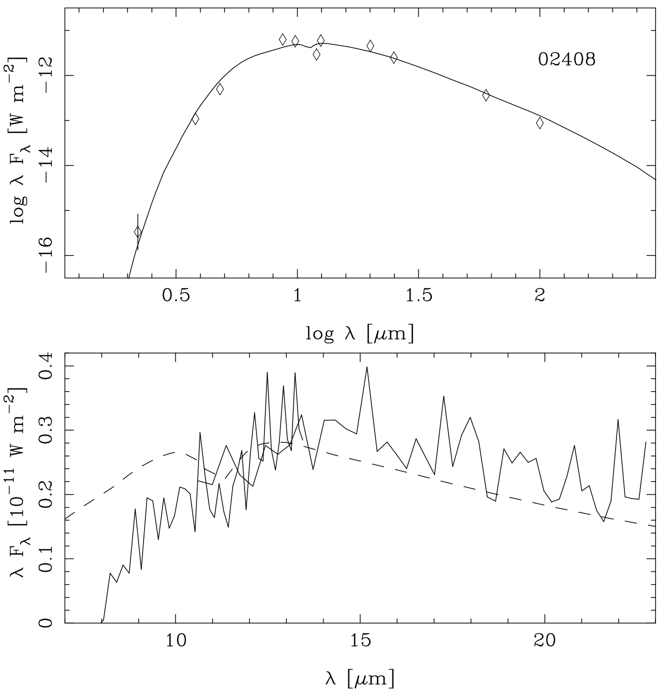

Fig. 10. Model fit to the observed SED and LRS spectrum. In the bottom panel the model is the dashed line, the LRS spectrum the solid line. This star is fitted with dust composed of 90% amorphous carbon and 10% silicon carbide.

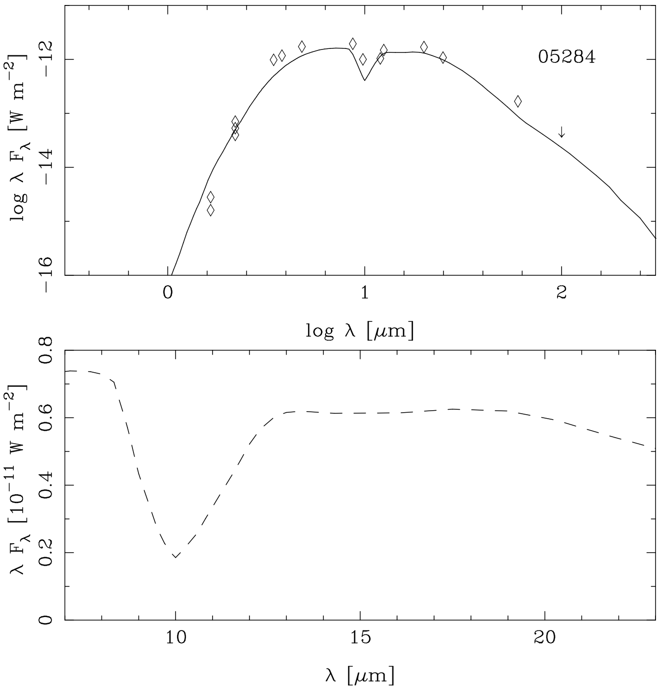

Fig. 11. As fig. 10. Silicate dust is used.

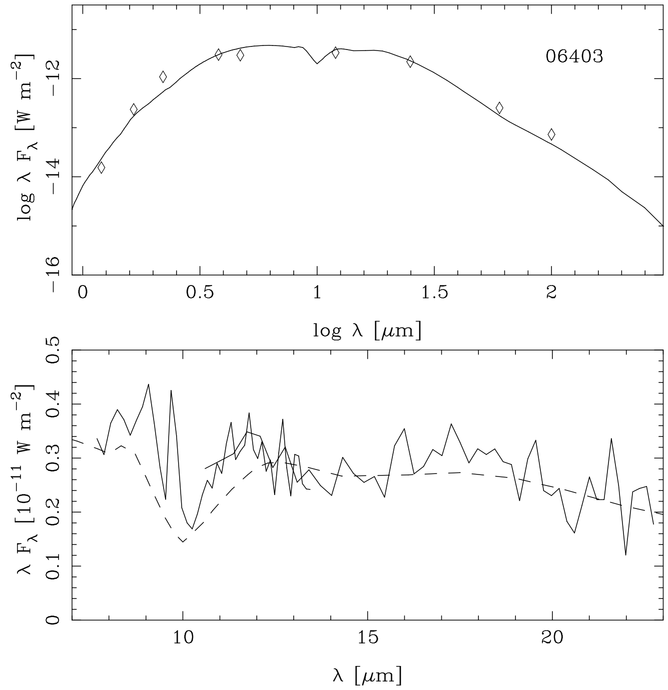

Fig. 12. As fig. 10. Silicate dust is used.

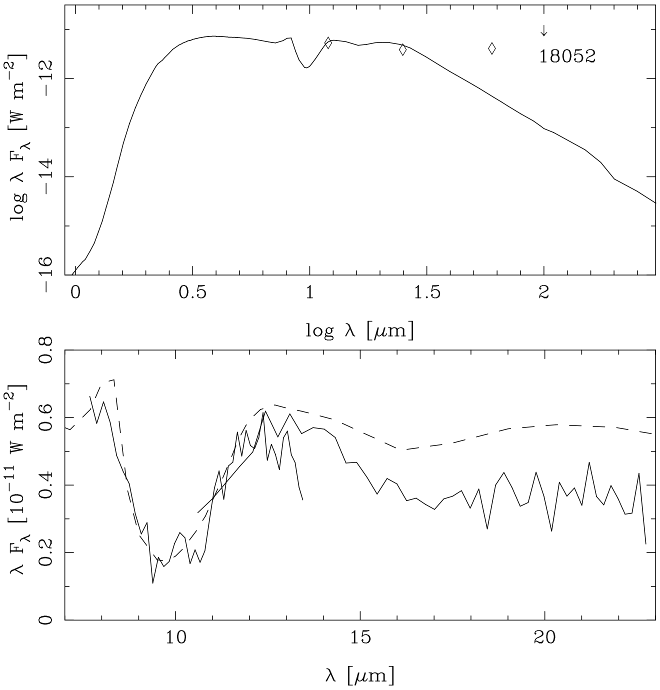

Fig. 14. As fig. 10. Silicate dust is used.

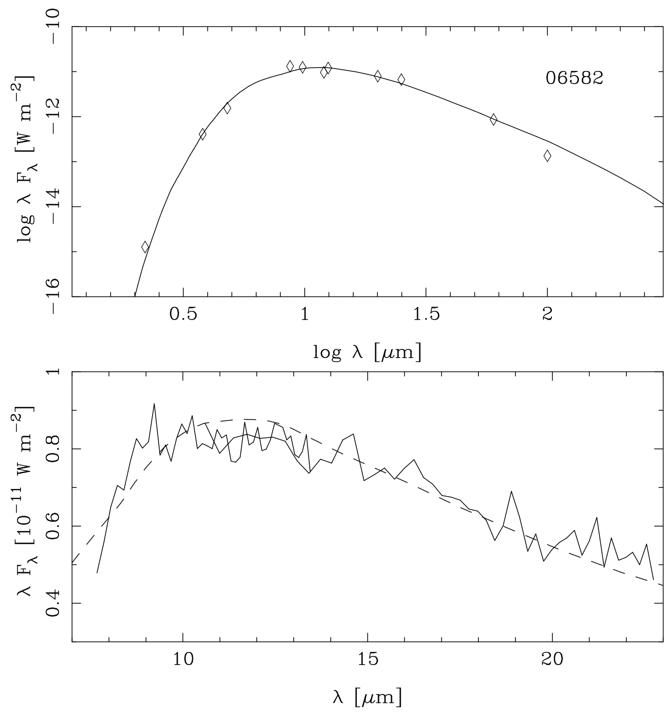

Fig. 13. As fig. 10. Pure amorphous carbon dust is used.

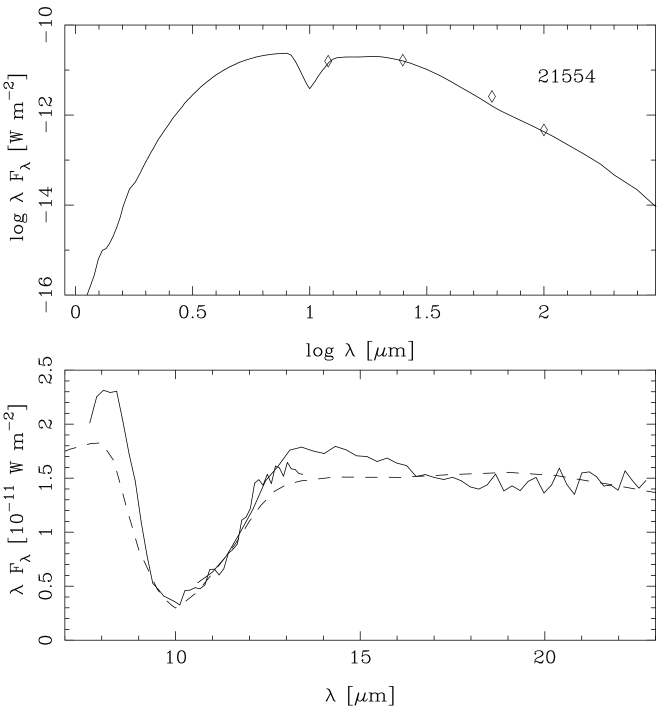

Fig. 15. As fig. 10. Silicate dust is used.

For most of the stars the distance is derived from the relation between the observed K-band magnitude and $M_{\rm K}$ as given by the $P - M_{\rm K}$-relation from Feast et al. (1989). No reddening corrections is applied, but should be negligible in the K-band for the distances under consideration here ($\lesssim$1 kpc for the stars this method was applied to). The observed K-band data was preferentially taken from the 2.2 μm IRC catalog. Observations from Catchpole et al. (1979), Epchtein et al. (1985), Fouqué et al. (1992) and Kerschbaum (private comm.) were also used. No attempt was made to bring these data to a common photometric system.

For 12 out of the sample of 35 C-stars, and 33 of the 62 O-rich stars under consideration a parallax measurement

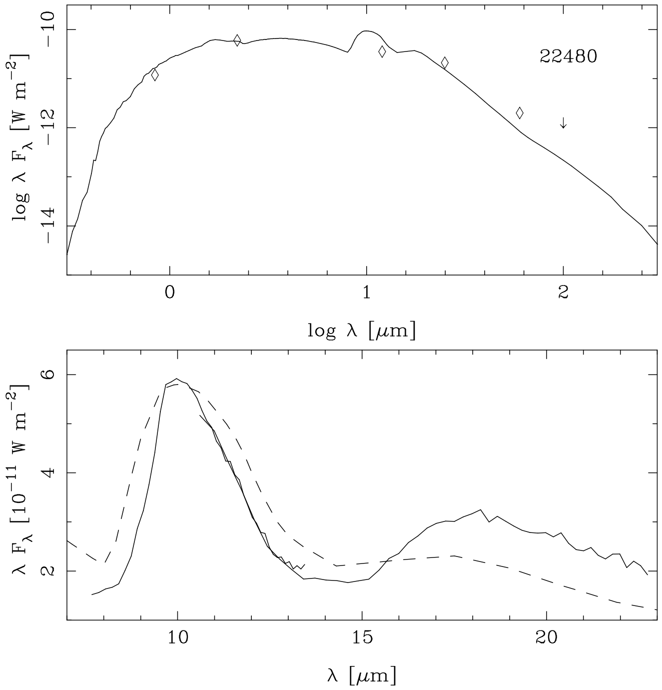

Fig. 16. As fig. 10. Silicate dust is used.

in the HIPPARCOS database (ESA, 1997) is available, but only for 2, respectively 10, objects, the parallax has been determined with an accuracy better than 50%, and only these cases have been included in Table 5. Additionally, for R Leo there is the ground-based parallax determination of Gatewood (1992; $\pi = 8.3 \pm 1.0$ mas) as well, which is more accurate than the HIPPARCOS parallax. One can compare the distances derived from the HIPPARCOS data and derived from the $P - M_{\rm K}$-relation. No infrared photometry is available for one star with a HIPPARCOS parallax. In 9 out of 11 cases, the distance based on the $P - M_{\rm K}$-relation is *larger* than the HIPPARCOS distance. For the stars with a poorly determined parallax ($(\sigma/\pi) > 0.21$, where σ is the error in the observed parallax) this is 7 out of 8. In one case the difference in distance is marginal, but for the other Miras it is a factor of 1.3, and then between factors of 1.9 and 4.4.

A neglect of reddening in our analysis can not be found responsible for this discrepancy. For distances $\lesssim$1 kpc, one expects visual extinctions $\lesssim$1 magnitude, which translates into $A_{\rm K} \lesssim$0.1 mag (corresponding to a $\lesssim$10% shift in distance). The $P - M_{\rm K}$-relation was applied to the Galaxy adopting a distance modulus to the LMC of 18.5. A larger distance modulus, as advocated by e.g. Feast & Catchpole (1997), would make the galactic stars only brighter and hence would increase the discrepancy. A possibility is that the LMC is actually closer than adopted here.

A natural explanation for the discrepancy is given by the so-called Lutz-Kelker bias (Lutz & Kelker 1973), and is related to the difference in sampled volume between a star with a parallax between $(\pi - \sigma)$ and (π), and (π) and $(\pi + \sigma)$ (also see Oudmaijer et al. 1998). One can introduce the concept of a 'most probable parallax' (e.g. Koen 1992), and its value depends on the underlying distribution of stars and additional constrains one may have (e.g. a luminosity function). In the case of no additional information and an uniform space density the most probable parallax is $(\frac{1}{2}\pi(1 + \sqrt{1 - 16(\frac{\sigma}{\pi})^2}))$ (Koen 1992). This is defined only for $(\sigma/\pi) < 0.25$. Although perhaps a meaningless comparison for one star only, application of this procedure to R Leo would change the observed HIPPARCOS parallax of 9.87 mas to a probable parallax of 7.62 mas, and the observed ground-based parallax from 8.3 mas to a probable parallax of 7.8 mas, in very good agreement with each other. Based on the 'most probable parallax' for the objects with $(\sigma/\pi) < 0.25$ we adopt the following distances: o Cet (140 pc), R Car (130 pc), and R Leo (130 pc). For the rest of the sample of stars with Hipparcos parallaxes we prefer to use the distance based on the $P - M_{\rm K}$-relation, because it is more reliable that the distance based on the parallax.

5.3. The gas mass loss rate from CO

Olofsson et al. (1993) give the following relation between the measured peak intensity of a CO line and the mass loss rate:

$$\dot{M}_{\rm g} = 1.4 \times \frac{T_{\rm mb}\, v_\infty^2\, D^2\, B^2}{2 \times 10^{19}\, f_{\rm CO}^{0.85}\, s(J)} \qquad (1)$$

where $\dot{M}_{\rm g}$ is in units of solar masses per year, $T_{\rm mb}$ in Kelvin, v_∞ in km s^{-1}, D the distance in parsec. B the FWHM size of the telescope beam in arcsec, $f_{\rm CO}$ the CO abundance relative to H_2, and $s(J)$ is a correction factor, equal to unity for the J = 1-0 transition and 0.6 for the J = 2-1 transition.

Equation (1) was calibrated for J = 2-1 and 1-0 transition but in view of the increasing number of available J = 3-2 observations, determination of s(3) would be useful. This was done on the basis of (rewriting Eq. 1 for given stellar parameters):

$$s(3) = s(2) \left(\frac{T_{3-2}}{T_{2-1}}\right) \left(\frac{B_{3-2}}{B_{2-1}}\right)^2 \qquad (2)$$

and only simultaneous observations with the same telescope were used in its application. Based on three stars observed with the CSO by Knapp et al. (1998) a geometric mean of s(3) = 0.43 is derived. Based on our own JCMT data for 7 stars we find s(3) = 0.43, and our own IRAM data on 6 stars results in s(3) = 0.24. The latter value is clearly off, and indicates a possible calibration error (a beam efficiency which is lower), or a contribution from the error beam. If the latter is true it should be less of a problem with the smaller JCMT and CSO telescopes. The IRAM J=3-2 data is not used to make an estimate of the mass loss rate, and in the other cases s(3) = 0.43 is used.

The gas mass loss rate is derived using both our CO results and the CO data in the papers listed in Table 1. Equation 1 was used with $f_{\rm CO} = 5 \times 10^{-4}$ for O-rich stars and 8×10^{-4} for C-stars to calculate the mass loss rate per unit distance. The gas mass loss rate listed in Table 5 is the range between minimum and maximum value in the case of multiple determinations.

The expansion velocity is required in this calculation and the finally adopted values are listed in Table 5. They are an average of the available CO data (ours and literature). When no, or only poor, CO data was available the expansion velocity is taken from OH and SiO data, when available, without any correction for the possible difference between the CO and OH/SiO expansion velocity. In other cases a value of 10 km s^{-1} is adopted.

5.4. The dust mass loss rate

The dust mass loss rate can be derived from a detailed modelling of the SED. This was done for most of the carbon-rich Miras in Groenewegen et al. (1998). In those cases the value they derived from the fit (their table 3) have been used, appropriately scaled for the slightly different velocities adopted in some cases. The same was done for AFGL 5076 and 5625 (Groenewegen 1995), and AFGL 5093 (Groenewegen et al. 1995), and the stars analysed in Sect. 5.1.

For the rest of the sample the relation between the 60 (or 25) μm flux and the dust mass loss rate is used. From Jura (1988) we have:

$$\dot{M}_{\rm d} = C\, v_{15}\, D^2\, L_4^{-0.5} \lambda_{10}^{0.5}\, \kappa_{150}^{-1}\, F(\lambda) \qquad (3)$$

where $\dot{M}_{\rm d}$ is the dust mass loss rate in units of solar masses per year, C is a constant, v_{15} is the dust expansion velocity in units of 15 km s^{-1}, D the distance in kpc, L_4 the luminosity in units of 10 000 L$_\odot$, λ_{10} the wavelength in units of 10 μm where the peak of the energy distribution occurs, and κ_{150} the opacity at 60 μm in units of 150 cm^{2}g^{-1}. $F(\lambda)$ is the excess emission at wavelength λ in Jansky. Jura (1988) uses $C = 7.7 \times 10^{-10}$ and $\lambda = 60$ μm.

It is clear that the *excess* emission should be used in Eq. 2, but in many applications, the *observed* flux has been used (see the discussion in Groenewegen & de Jong 1998). Following that paper we have corrected for the photospheric contribution to the observed flux based on a simple radiative transfer model. This correction is explained for O-rich stars in Groenewegen & de Jong (1998; their Fig. 4). In the case of carbon stars we performed similar calculations, which are based on a dust shell composed of amorphous carbon mixed with 10% silicon carbide around a central star with a blackbody temperature of 2500 K. The inner dust temperature was set at 1200 K. Shells of increasing optical depth were calculated and the fraction of excess emission determined as a function of S_{12}/S_{25} ratio (see Fig. 17).

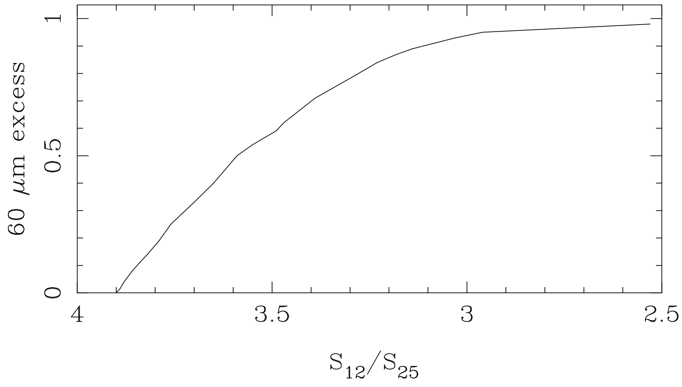

Fig. 17. Fraction of excess emission at 60 μm, as a function of flux-ratio at 12 and 25 μm, for the model described in Sect 5.4.

The constant C in Eq. 3 at $\lambda = 60$ μm is 1.34×10^{-9} for O-rich star models (Groenewegen & de Jong 1998) and 5.35×10^{-10} for C-star models. At $\lambda = 25$ μm these numbers are 2.43×10^{-10} and 1.49×10^{-10}, respectively[1].

6. Results of the analysis

In this section some implications are discussed. Figure 18 shows the relation between the gas mass loss rate based on the analysis described in the previous sections, and from the combination of the dust mass loss rate derived from model fitting of the SEDs and the theory of radiation pressure on dust (Groenewegen et al. 1998) for 19 C-stars in common. The results are in perfect agreement for mass loss rates higher than $10^{-5.5}$ M$_\odot$ yr^{-1}, and there is some indication that the mass loss rate from CO is slightly less that that derived in Groenewegen et al. (1998) for small mass loss rates. An unweighted least-squares fit gives:

$$\log \dot{M}(\text{previous}) = (0.85 \pm 0.09) \times \log \dot{M}(\text{this paper}) - (0.77 \pm 0.55);\ \sigma = 0.24. \qquad (4)$$

This implies that two completely independent methods give mass loss rates that agree to better than a factor of two, and that over a wide range of mass loss rates.

Figure 19 shows the relation between mass loss rate and pulsation period for the present sample. The solid line is the relation for C-Miras derived in Groenewegen et al. (1998). It seems that at the shorter period the mass loss rates for the O-rich stars are significantly smaller than for C-stars, and they do not follow the relation for C-stars found by Groenewegen et al. (1998). Although a detailed comparison will be deferred to a future paper, we note here that some semi-regulars (SRs) of spectral type S

[1] Note that the number of 7.67×10^{-11} in Groenewegen et al. (1998) is incorrect. Since the relation at 25 μm was not actually used this has no consequences on any of the results in that paper.

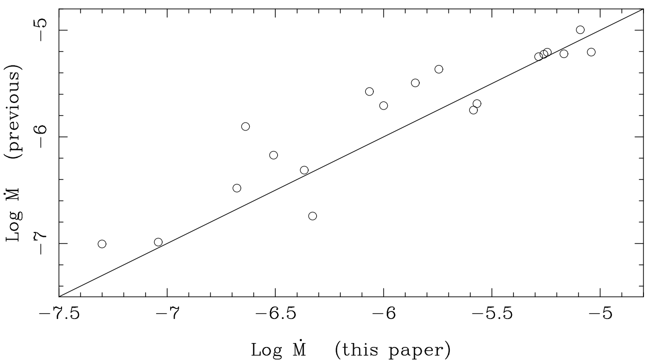

Fig. 18. Comparison between the total mass loss rates, for carbon stars only, derived in this paper (based on CO data), and in Groenewegen et al. (1998) based on the dust mass loss rate in conjunction with radiation driven wind theory. The solid line is the one-to-one relation.

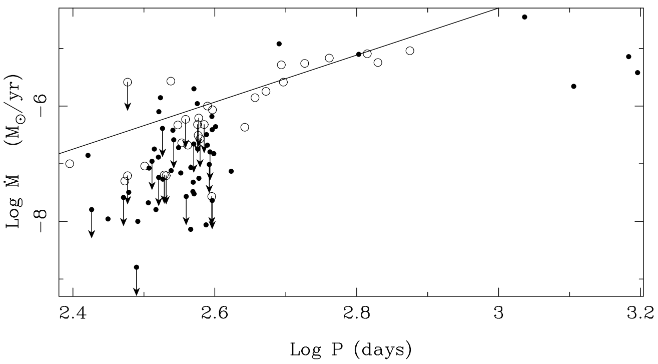

Fig. 19. The relation between Log (Period) and Log (total mass loss rate). ∘ = Carbon stars, • = O-rich stars. The solid line is the relation derived in Groenewegen et al. (1998) for C-Miras.

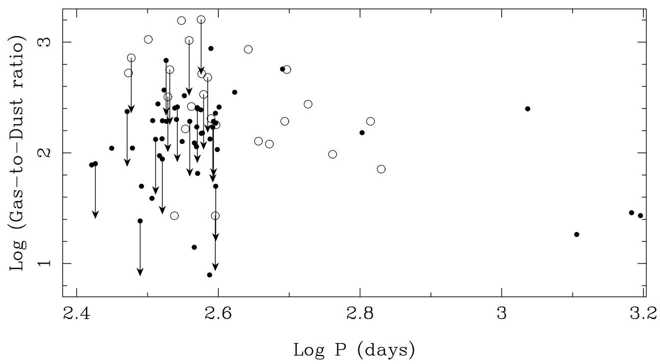

Fig. 20. The relation between Log (Period) and Log (gas-to-dust ratio). Symbols as in previous figure.

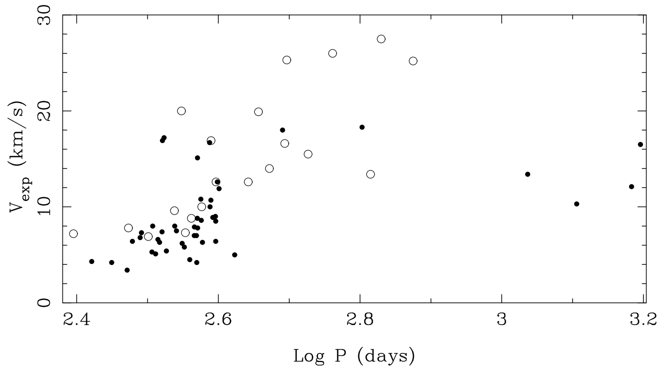

Fig. 21. The relation between Log (Period) and expansion velocity. Symbols as in previous figure.

(see Groenewegen & de Jong 1998), and O-rich SRs (Kerschbaum et al. 1996) have mass loss rates between 10^{-8} and 10^{-7} $M_\odot\,yr^{-1}$ at periods between 100 and 250 days. A second implication of the present data is that the mass loss rate seems to level off above $P = 500$ days at a level near 10^{-5} $M_\odot\,yr^{-1}$, independent of chemical type.

Figure 20 shows the gas-to-dust ratio as a function of pulsation period. A similar trend is observed in the gas–to dust ratio. At short periods the gas-to-dust ratio of C-stars seems to be higher than for the corresponding O-rich stars. At longer periods, there seems to be no dependence on chemical type, and the gas-to-dust ratio decreases.

Figure 21 shows the expansion velocity as a function of period. Particularly for O-rich stars an upper limit of 18 km s^{-1} is observed around $P = 600$ days in the present sample with decreasing expansion velocities towards shorter and longer periods. Similar upper limits on the expansion velocity of O-rich stars of about 20 km s^{-1} can be observed in Loup et al. (1993), Groenewegen & de Jong (1998), Kerschbaum & Olofsson (1999). Note that some known O-rich sources in our sample have larger expansion velocities, but they are known supergiants, or no period is known. The upper limit on the expansion velocity is in qualitative agreement with the calculations presented by Habing et al. (1994) for AGB stars which predict a maximum attainable expansion velocity for a mass loss rate of about 5×10^{-6} $M_\odot\,yr^{-1}$ in O-rich stars. Their models also predict that the expansion velocity in C-stars reaches larger values, which is indeed confirmed from our data (also see Groenewegen & de Jong 1998).

We consider the present discussion of the results as preliminary. In a future publication we will combine the CO data, and the derived mass loss rates with other recent publication on CO measurements in MS- and S-stars (Groenewegen & de Jong 1998), Semi-Regular and Irregular variables (Kerschbaum & Olofsson 1998, 1999), and other literature data. Using this much larger dataset it should be possible to see if the correlations presented here hold for the other categories of variable stars, and from that also gain insight into the *evolutionary connection* between the Carbon-, S-type and Oxygen-rich Lb, SR and

Mira variables, which is yet not possible from the present limited dataset.

Acknowledgements. We would like to thank Franz Kerschbaum (Vienna) for providing us with unpublished IR photometry of RZ Mus. This research has made use of the SIMBAD database, operated at CDS, Strasbourg, France. Felipe Mac-Aulife and Francisco Azagra (SEST staff) are thanked for doing some of the September 1996 and September 1998 SEST observations, respectively.

References

Arenou F., Grenon M., Gomez A., 1992, A&A 258, 104
Benson P.J., Little-Marenin I.R., 1996, ApJS 106, 579
Bieging J.H., Latter W.B., 1994, ApJ 422, 765
Bieging J.H., Knee L.B.G., Latter W.B., Olofsson H., 1999, A&A 339, 811
Blommaert J.A.D.L., van der Veen W.E.C.J., Habing H.J., 1993, A&A 267, 39
Blommaert J.A.D.L., van Langevelde H.J., Michiels W.F.P., 1994 A&A 287, 479
Bujarrabal V., Fuente A., Omont A., 1994, A&A 285, 247
Catchpole R.M., Robertson B.S.C., Lloyd Evans T.H.H., Feast M.W., Glass I.S., Carter B.S., 1979, SAAO Circ. 1, 61
Cho S.-H., Kaifu N., Ukita N., 1996, A&AS 115, 117
David P., Papoular R., 1990, A&A 237, 425
Dominik C., Gail H.-P., Sedlmayr E., Winters J.M., 1990, A&A 240, 365
Dorschner J., Begemann B., Henning Th., Jager C., Mutschke H., 1995, A&A 300, 503
Duflot M., Figon P., Meyssonnier N., 1995, A&AS 114, 269 (used is version 6 of their catalog (march 1998), available through the CDS)
Engels D., 1994, A&A 285, 497
Epchtein N., Matsuura O.T., Braz M.A., Lépine J.R.D, Picazzio E., et al., 1985, A&AS 61, 203
ESA, "The Hipparcos and Tycho Catalogues", 1997, ESA SP-1200
Feast M.W., Catchpole R.M., 1997, MNRAS 286, L1
Feast M.W., Glass I.S., Whitelock P.A., Catchpole R.M., 1989, MNRAS 241, 375
Forveille T., Guilloteau S., Lucas R., 1990, IRAM publication
Fouqué P., Le Bertre T., Epchtein N., Guglielmo F., Kerschbaum F., 1992, A&AS 93, 151
Garcia-Lario P., Manchado A., Pych W., Pottasch S.R., 1997, A&AS 126, 479
Gatewood G., 1992, PASP 104, 23
Groenewegen M.A.T., 1993, Chapter 5, Ph.D. thesis, University of Amsterdam
Groenewegen M.A.T., 1995, A&A 293, 463
Groenewegen M.A.T., 1999, in: "IAU Symposium 191: AGB stars", Eds. T. Le Bertre, A. Lebre and C. Waelkens, Astr. Soc. of the Pacific, p. 535
Groenewegen M.A.T., Baas F., de Jong T., Loup C., 1996, A&A 306, 241
Groenewegen M.A.T., de Jong T., 1998, A&A 337, 797
Groenewegen M.A.T., de Jong T., van der Bliek N.S., Slijkhuis S., Willems F.J., 1992, A&A 253, 150
Groenewegen M.A.T., Smith C.H., Wood P.R., Omont A., Fujiyoshi T., 1995, ApJ 449, L119
Groenewegen M.A.T., Whitelock P.A., Smith C.H., Kerschbaum F., 1998, MNRAS 293, 18
Groenewegen M.A.T., Whitelock P.A., 1996, MNRAS 281, 1347
Habing H.J., Tignon J., Tielens A.G.G.M., 1994, A&A 286, 523
Haikala L.K., 1990, A&AS 85, 875
Haikala L.K., Nyman L.-Å., Forsström V., 1994, A&AS 103, 107
Han F., Mao R.Q., Lu J., Wu Y.F., Sun J., Wang J.S., Pei C.C., Fan Y., Tang G.S.,Ji H.R., 1998, A&AS 127, 181
Jiang B.W., Deguchi S., Hu J.Y., Yamamura I., Nakada Y., Cho S.H., Yamagata T., 1996, ApJS 106, 463
Jiang B.W., Deguchi S., Hu J.Y., Yamashita T., Nishihara E., Matsumoto S., Nakada Y., 1997, AJ 113, 1315
Jones T.J., Bryja C.O., Gehrz R.D., Harrison T.E., Johnson J.J., et al., 1990, ApJS 74, 785
Jones T.W., Merrill K.M., 1976, ApJ 209, 509
Josselin E., Loup C., Omont A., Barnbaum C, Nyman L-A, Sèvre F., 1998, A&AS 129, 45
Joyce R.R., Merrill K.M., Gillett F.C., 1999, in preparation
Jura M., 1988, ApJS 66, 33
Kerschbaum F., Olofsson H., Hron J., 1996, A&A 311, 273
Kerschbaum F., Olofsson H., 1998, A&A 336, 654
Kerschbaum F., Olofsson H., 1999, A&AS 122, 167
Kholopov P.N., Samus N.N., Frolov M.S., et al., 1985, General Catalog of Variable Stars (GCVS), Nauka, Moscow
Knapp G.R., Young K., Lee E., Jorissen A., 1998, ApJS 117, 209
Koen C., 1992, MNRAS 256, 65
Le Bertre T., 1992, A&AS 94, 377
Lewis B.M., 1997, AJ 114, 1602
Likkel L., Miao Y, 1996, AJ 112, 301
Loup C., Forveille T., Omont A., Paul J.F., 1993, A&AS 99, 291
Lutz T.E., Kelker D.H., 1973 PASP 85, 573
Margulis M., van Blerkom D.J., Snell R.L., Kleinmann S.G., 1990, ApJ 361, 673
Neri R., Kahane C., Lucas R., Bujarrabal V., Omont A., 1998, A&AS 130, 1
Nyman L.-A., Booth R.S., Carlström U., et al., 1992, A&AS 93, 121
Nyman L.-A., Hall P.J., Olofsson H., 1998, A&AS 127, 185
Olofsson H., Eriksson K., Gustafsson B., Carlström U., 1993, ApJS 87, 267
Olofsson H., Lindqvist M., Nyman L-A., Winnberg A., 1998, A&A 329, 1059
Oudmaijer, R.D., M.A.T. Groenewegen, H. Schrijver, 1998, MNRAS 294, L41
Sahai R., Liechti S., 1995, A&A 293, 198
Speck A.K., Barlow M.J.,Skinner C.J., 1997, MNRAS 288, 431
Stanek K.Z, Kanpp G.R., Young K., Phillips T.G., 1995, ApJS 100, 169
Stephenson C.B., 1989, Pub. Warner and Swasey Obs, vol. 3, No. 2
Suh, K.-W., 1999, MNRAS 304, 389
Te Lintel Hekkert P., Caswell J.L., Habing H.J., Haynes R.F., Norris R.P., 1991, A&AS 90, 327
van Langevelde H.J., van der Heiden R., Schooneveld C., 1990, A&A 239, 193

Table 5. Derived parameters

Name	Parallax (mas)	Lum. ($L_\odot$)	D (kpc)	method	v_∞ (km/s)	$\dot{M}_{dust}$ ($M_\odot$ yr^{-1})	$\dot{M}_{gas}$ ($M_\odot$ yr^{-1})	Ψ
V390 Cas		5400	3.10	4b	(10)	5.7 $\times 10^{-10}$	<5.9 $\times 10^{-7}$	<1035
PT Cas		4400	5.68	4b	(10)	0.0	<2.6 $\times 10^{-6}$	–
CN Per		5720	3.09	1	(10)	1.0 $\times 10^{-9}$	<4.8 $\times 10^{-7}$	<480
R For		5790	0.60	1	16.9	4.9 $\times 10^{-9}$	0.51-1.9 $\times 10^{-6}$	204
AFGL 5076		7050	3.99	8	19.7	4.9 $\times 10^{-7}$	4.1-6.6 $\times 10^{-5}$	104
IRAS 02408+5458		5700	5.3	9	11.0	3.5 $\times 10^{-7}$	1.5-1.7 $\times 10^{-5}$	46
Y Per		3700	1.04	1	7.2	0.0	1.0 $\times 10^{-7}$	∞
GY Per		5600	3.25	4b	(10)	2.6 $\times 10^{-11}$	<6.2 $\times 10^{-7}$	<23800
R Ori		5630	2.2	1	10.0	6.0 $\times 10^{-10}$	3.1 $\times 10^{-7}$	517
UV Aur		5800	0.85	1	(10)	1.0 $\times 10^{-9}$	<2.7 $\times 10^{-8}$	<27
V Aur		5240	1.16	1	20.0	3.0 $\times 10^{-10}$	4.7 $\times 10^{-7}$	1570
ZZ Gem		4690	1.32	1	6.9	8.6 $\times 10^{-11}$	0.76-1.1 $\times 10^{-7}$	1060
AFGL 935		7430	2.00	1	16.6	2.7 $\times 10^{-8}$	1.8-6.2 $\times 10^{-6}$	193
AFGL 971		9910	1.55	1	13.4	4.2 $\times 10^{-8}$	0.16-1.3 $\times 10^{-5}$	193
CL Mon		7470	0.82	1	25.3	4.6 $\times 10^{-9}$	2.1-3.1 $\times 10^{-6}$	565
IRAS 06582+1507		6500	3.5	9	15.5	4.5 $\times 10^{-7}$	1.1-4.3 $\times 10^{-5}$	53
R CMi		5010	0.86	1	(10)	2.0 $\times 10^{-10}$	<6.4 $\times 10^{-8}$	<320
R Vol		6800	0.75	1	19.9	1.1 $\times 10^{-8}$	0.8-2.4 $\times 10^{-6}$	127
VX Gem		5650	1.62	1	(10)	8.0 $\times 10^{-10}$	<2.7 $\times 10^{-7}$	<340
C1698					(10)			
R Pyx		5420	1.20	1	8.8	8.0 $\times 10^{-10}$	1.8-2.5 $\times 10^{-7}$	263
V Cru		5600	1.33	1	(10)	3.0 $\times 10^{-10}$	<4.8 $\times 10^{-7}$	<1600
V CrB		5310	0.71	1	7.3	1.4 $\times 10^{-9}$	0.49-2.9 $\times 10^{-7}$	164
V Oph	3.65 ± 1.23	4390	0.68	1	7.8	9.5 $\times 10^{-11}$	3.7-6.7 $\times 10^{-8}$	526
AFGL 2310		8720	0.81	1	26.0	7.0 $\times 10^{-8}$	5.1-7.6 $\times 10^{-6}$	97
AFGL 2368		10280	0.88	1	27.5	8.0 $\times 10^{-8}$	0.43-1.1 $\times 10^{-5}$	71
R Cap		5120	1.47	1	9.6	1.0 $\times 10^{-7}$	1.0-8.0 $\times 10^{-6}$	27
AFGL 2686		11440	1.08	1	25.2	1.0 $\times 10^{-9}$	0.76-1.2 $\times 10^{-5}$	910
V1549 Cyg		8030	1.32	1	15.5	2.0 $\times 10^{-8}$	4.2-6.1 $\times 10^{-6}$	275
AX Cep		5890	1.05	1	12.6	4.8 $\times 10^{-9}$	0.85-1.6 $\times 10^{-6}$	179
AFGL 5625		7050	1.47	8	18.0	5.8 $\times 10^{-7}$	0.60-2.2 $\times 10^{-5}$	20
CIT 13		7050	0.72	1	14.0	1.5 $\times 10^{-8}$	1.1-3.4 $\times 10^{-6}$	120
RZ Peg	3.54 ± 1.36	6570	1.23	1	12.6	5.0 $\times 10^{-10}$	4.3 $\times 10^{-7}$	860
AO Lac		4400		4	(10)	8.6 $\times 10^{-11}$/kpc^2	<6.2 $\times 10^{-14}$/pc^2	<720
LS Cas		5000		4	(10)	1.1 $\times 10^{-10}$/kpc^2	<6.2 $\times 10^{-14}$/pc^2	<560
S Scl		6600	0.46	5b	4.5	1.4 $\times 10^{-10}$	<2.7 $\times 10^{-8}$	<193
AFGL 230		56 800	2.9	2	12.1	2.5 $\times 10^{-7}$	3.1-8.9 $\times 10^{-6}$	29
o Cet	7.79 ± 1.07	3700	0.14	5a	16.9	4.1 $\times 10^{-9}$	0.41-2.1 $\times 10^{-6}$	195
R Cet		2600	0.76	5c	8.7	1.1 $\times 10^{-9}$	1.3-2.9 $\times 10^{-7}$	118
R Tri		4600	0.50	5b	(10)	2.0 $\times 10^{-10}$	<1.6 $\times 10^{-8}$	<80
U Ari		6700	0.76	5b	4.2	2.8 $\times 10^{-10}$	0.19-1.2 $\times 10^{-7}$	171
AFGL 5093		15 800	3.2	7	10.3	1.2 $\times 10^{-7}$	1.7-2.5 $\times 10^{-6}$	18
AFGL 5097		36 400	6.5	3	12.3	1.4 $\times 10^{-7}$	4.6-7.2 $\times 10^{-6}$	41
RT Eri		6700	0.41	5b	7.0	2.9 $\times 10^{-10}$	2.6-4.1 $\times 10^{-8}$	114
U Hor		6300	0.94	5b	(10)	1.0 $\times 10^{-9}$	<2.6 $\times 10^{-7}$	<260
W Eri		6900	0.93	5b	8.6	1.2 $\times 10^{-9}$	0.81-3.8 $\times 10^{-7}$	150
RS Eri		5200	0.64	5b	3.4	1.1 $\times 10^{-10}$	<2.6 $\times 10^{-8}$	240
R Tau		5700	0.59	5b	5.3	5.4 $\times 10^{-10}$	1.5-6.5 $\times 10^{-8}$	39
BD Eri		6000	0.90	5b	(10)	6.0 $\times 10^{-10}$	<4.1 $\times 10^{-7}$	<680
RX Tau		5900	0.70	5b	(10)	6.6 $\times 10^{-10}$	<5.8 $\times 10^{-8}$	<88
R Cae		7200	0.50	5b	8.9	5.7 $\times 10^{-10}$	<9.7 $\times 10^{-8}$	<170
T Lep		6700	0.43	5c	7.0	5.2 $\times 10^{-10}$	7.3 $\times 10^{-9}$	14
NV Aur		5600	1.0	3	18.3	5.2 $\times 10^{-8}$	0.61-1.2 $\times 10^{-5}$	152
U Dor		7300	0.76	5c	9.0	2.9 $\times 10^{-9}$	5.1-6.8 $\times 10^{-7}$	228
AFGL 712		73 300	8.0	3	13.4	1.4 $\times 10^{-7}$	2.3-5.2 $\times 10^{-5}$	250
IRAS 05284+1945		2200	5.0	9	14.0	8.2 $\times 10^{-8}$	4.7-6.7 $\times 10^{-6}$	70
RT Lep		7400	0.92	5b	11.9	1.7 $\times 10^{-9}$	4.4 $\times 10^{-7}$	260
U Ori		6700	0.31	5b	7.9	7.0 $\times 10^{-10}$	0.12-2.8 $\times 10^{-7}$	123

Table 5. Continued

Name	Parallax (mas)	Lum. ($L_\odot$)	D (kpc)	method	v_∞ (km/s)	$\dot{M}_{dust}$ ($M_\odot$ yr^{-1})	$\dot{M}_{gas}$ ($M_\odot$ yr^{-1})	Ψ
IRAS 06403−0138		1120	2.0	9	10.0	2.5×10^{-8}	3.3×10^{-7}	13
IRAS 07113−2747		35 100	11.0	3	8.1	1.3×10^{-7}	1.4-1.5 $\times 10^{-5}$	112
AS Pup	3.95 ± 1.02	5800		5	5.1	8.3×10^{-10}/kpc^2	<1.1 $\times 10^{-13}$/pc^2	<133
R Car	7.84 ± 0.83	5400	0.13	5a	6.8	6.6×10^{-11}	<1.6 $\times 10^{-9}$	24
X Hya		5300	0.54	5b	6.4	2.9×10^{-10}	2.2-4.8 $\times 10^{-8}$	110
R LMi		6800	0.29	5b	7.8	4.6×10^{-10}	1.8-5.2 $\times 10^{-8}$	65
R Leo	9.87 ± 2.07	5500	0.13	5a	7.3	2.0×10^{-10}	0.35-1.9 $\times 10^{-8}$	50
W Vel	3.56 ± 1.69	7300	0.55	5b	6.4	4.6×10^{-10}	<2.3 $\times 10^{-8}$	<50
RZ Mus		6000	1.11	5b	17.2	3.8×10^{-9}	0.78-2.6 $\times 10^{-6}$	360
AQ Cen		7100	0.86	5b	10.0	2.4×10^{-9}	3.2×10^{-7}	133
RU Hya		5900	0.73	5b	7.4	9.7×10^{-10}	1.3×10^{-7}	134
RS Vir		6400	0.74	5b	6.2	1.5×10^{-9}	0.99-3.8 $\times 10^{-7}$	127
Y Lup		7300	0.67	5b	12.6	1.4×10^{-9}	1.5×10^{-7}	107
S Ser	3.70 ± 1.62	6800	0.79	5b	8.8	8.6×10^{-10}	<2.2 $\times 10^{-7}$	<256
RS Lib		3600	0.22	5b	5.0	8.2×10^{-11}	1.8×10^{-8}	220
BG Ser		2200	0.24	5	11.0	2.0×10^{-10}	<2.8 $\times 10^{-6}$	<14 400
R Ser	3.58 ± 1.51	6500	0.37	5b	5.8	2.1×10^{-10}	0.14-1.0 $\times 10^{-7}$	330
RR Sco	2.84 ± 1.30	4900	0.28	5b	4.2	1.0×10^{-10}	1.1×10^{-8}	110
RW Sco		7200	0.70	5b	10.7	2.4×10^{-10}	2.1-2.2 $\times 10^{-7}$	875
V545 Oph		3700		5	9.3	1.9×10^{-9}/kpc^2	2.1×10^{-13}/pc^2	111
V438 Sco		7200	0.87	5b	(10)	8.3×10^{-10}	<1.6 $\times 10^{-7}$	193
WY Her		6900	1.53	5b	10.8	4.5×10^{-9}	1.1×10^{-6}	244
OH 10.1−0.1		30 000	8.0	9	27.3	3.1×10^{-7}	<6.0 $\times 10^{-5}$	<194
X Oph		5900	0.23	5b	6.3	1.7×10^{-10}	1.6-1.7 $\times 10^{-8}$	94
V342 Sgr		6800	0.67	5b	15.1	8.0×10^{-9}	1.5-2.4 $\times 10^{-6}$	250
W Aql		10 380	0.68	6	18.0	2.1×10^{-8}	0.68-2.4 $\times 10^{-5}$	571
RT Aql		5800	0.67	5b	6.6	6.5×10^{-10}	0.83-2.1 $\times 10^{-7}$	277
BG Cyg	3.96 ± 1.41	7900	0.77	5b	5.0	2.1×10^{-10}	7.4×10^{-8}	350
RR Sgr		6000	0.51	5b	5.4	2.8×10^{-10}	5.4×10^{-8}	193
RR Aql		7300	0.55	5b	8.5	2.1×10^{-9}	2.1-6.0 $\times 10^{-7}$	185
Z Cyg		4500	0.94	5b	4.3	1.8×10^{-9}	0.37-1.8 $\times 10^{-7}$	78
RU Cap		6300	1.42	5c	7.5	1.9×10^{-9}	3.8×10^{-7}	200
TU Peg		5700	0.63	5b	8.0	4.3×10^{-10}	8.4×10^{-8}	195
IRAS 21554+6204		7560	2.5	9	16.6	2.5×10^{-7}	1.0-2.8 $\times 10^{-5}$	72
AFGL 2885		27 400	2.30	2	16.5	1.4×10^{-7}	2.2-5.7 $\times 10^{-6}$	27
AFGL 2968		140 000	5.0	9	26.4	1.4×10^{-7}	1.4-7.2 $\times 10^{-5}$	350
R Peg		6900	0.46	5b	6.3	3.7×10^{-10}	1.3-8.0 $\times 10^{-8}$	151
W Peg	3.46 ± 1.38	6200	0.31	5b	8.0	3.0×10^{-10}	6.1-7.6 $\times 10^{-8}$	253
R Aqr		7100	0.23	5b	16.7	1.1×10^{-9}	8.7×10^{-9}	7.9

Methods:
1) Luminosity from the C-star PL-relation of Groenewegen & Whitelock (1996). Distance obtained from detailed modelling of the SED (Groenewegen et al. 1998).
2) Distance from the 'phase-lag' method (van Langevelde et al. 1990), luminosity from Blommaert et al. (1994), based on integration under the SED.
3) Distance from kinematics (Blommaert et al. 1994) and luminosity by the same authors, based on integration under the SED.
4) Luminosity from the C-stars PL-relation of Groenewegen & Whitelock (1996); 4b) distance from the observed K-band magnitude and a Period-M_K relation (Groenewegen & Whitelock 1996)
5) Luminosity from the PL-relation (Feast et al. 1989) of O-rich Miras in the LMC for a distance modulus of 18.5. Distance from: (5a) most probable parallax (see text); (5b) from the observed K-band magnitude and a Period-M_K relation (Feast et al. 1989); (5c) as quoted by Whitelock et al. (1995).
6) From Groenewegen & de Jong (1998).
7) Distance from the 'phase-lag' method (van Langevelde et al. 1990), luminosity scaled from Groenewegen et al. (1995) based on model fitting of the SED. The dust mass loss rate is also derived from the model fitting, appropriately scaled from Groenewegen et al. (1995).
8) Luminosity adopted, distance and dust mass loss rate from model fitting to the SED (Groenewegen 1995), scaled to the adopted velocity.
9) Distance from kinematics (or adopted for IRAS 05285+1945; OH 10.1–0.1 assumed to be near the galactic center at 8.0 kpc), luminosity and dust mass loss from model fitting of the SED (this paper, Sect.5.1).

Volk K., Kwok S., Woodsworth A.W., 1993, ApJ 402, 292
Whitelock P.A., 1990, in: "Confrontation between stellar pulsation and evolution", ASP Conf. Ser. 11, eds. C. Cacciari and G. Clementini, p. 365
Whitelock P.A., Menzies J., Feast M.W., Marang F., Carter B., Roberts G., Catchpole R., Chapman J., 1994, MNRAS 267, 711
Whitleock P.A., Menzies J., Feast M.W., Catchpole R., Marang F., Carter B., 1995, MNRAS 276, 219
Young K., 1995, ApJ 445, 872